



*University of Padova*

*Department of Information Engineering*
*Master's Degree in Bioengineering*

# Mathematical description of tumour re-oxygenation from repeated functional imaging: the impact of the choice of the reference region and modeling parameters

*Author:*
**Filippo Schiavo**

*Supervisor at University of Padova:*
**Prof. Alfredo Ruggeri**

*Supervisors at Stockholm University:*
**Dr. Marta Lazzeroni**
**Prof. Iuliana Toma-Dasu**

10th September 2018

Academic Year 2017-2018

## Abstract

Hypoxia is one of the most probable cause of treatment failure of radiotherapy for Head and Neck Cancer, due to the proven higher resistance of cells to radiation when oxygen supply is reduced. The detection of tumor hypoxia, together with its specific localization and evolution in time could be fundamental factors for patients classification between responders and non-responders to the standard radiotherapy. Positron Emission Tomography with $^{18}$F-fluoromisonidazole ($^{18}$F-FMISO), a radiotracer specific for hypoxia detection, is obtaining promising results in treatment outcome prognosis and could obtain further validation for dose painting in the future.

In this thesis, thirty patients affected by Head and Neck Squamous Cell Carcinoma treated with concurrent chemoradiotherapy and repeatedly imaged with FMISO PET were analyzed. In particular, the uptake values in the images were converted in maps of oxygen tension, closely connected to cells radiosensitivity, by the use of a sigmoidal function. As a well-oxygenated volume is required as reference, the first aim of this study is the determination of the influence of choosing different references in terms of localization and $pO_2$ level. The second objective consists in the study of a method for a parametric characterization of the re-oxygenation process, based on a recently proposed algorithm.

The study revealed the possibility of using as reference volume the deep neck muscle, with 29 mmHg as associated oxygenation level, while the re-oxygenation mechanism has been characterized by a system, where the shape or the parameters of the response could potentially predict the clinical course of the disease.

# Contents

# List of Figures

# Abbreviations

**3D-CRT:** Three-Dimensional Conformal RadioTherapy

**ATSM:** diAceTyl-bis($N^4$)-methylthioSeMicarbazone

**BED:** Biologically Effective Dose

**BOLD-MRI:** Blood Oxygenation Level Dependent - Magnetic Resonance Imaging

**CBCT:** Cone-Beam Computer Tomography

**CT:** Computer Tomography

**CTV:** Clinical Target Volume

**DIR:** Deformable Image Registration

**DPBC:** Dose Painting By Contours

**DPBN:** Dose Painting By Numbers

**FAZA:** FluoroAZomycin-Arabinofuranoside

**FDG:** FluoroDeoxyGlucose

**FETA:** FluoroETAnidazole

**FETNIM:** FluoroEryThroNitroIMidazole

**FMISO:** FluoroMISOnidazole

**GKI:** Gamma Knife Icon

**GTV:** Gross Tumor Volume

**HNC:** Head and Neck Cancers

**HTV:** Hypoxic Target Volume

**HX4:** Flortanidazole

**HNSCC:** Head and Neck Squamous Cell Carcinoma

**IGRT:** Image-Guided RadioTherapy

**IMRT:** Intensity-Modulated RadioTherapy

**ITV:** Internal Target Volume

**LET:** Linear Energy Transfer

**LQ:** Linear Quadratic

**MRI:** Magnetic Resonance Imaging

**NPC:** NasoPharynx Cancer

**NSCLC:** Non-Small-Cell Lung Carcinoma

**NTCP:** Normal Tissue Complication Probability

**OAR:** Organ At Risk

**OER:** Oxygen Enhancement Ratio

**OSCC:** Oral Squamous Cell Carcinoma

**PET:** Positron Emission Tomography

**PRV:** Planning organ at Risk Volume

**PTV:** Planning Target Volume

**ROS:** Reactive Oxygen Species

**RT:** Radiation Therapy

**SBRT:** Stereotactic Body RadioTherapy

**SLD:** Sub-Lethal Damages

**SRS:** Stereotactic RadioSurgery

**STV:** Systematic Target Volume

**SUV:** Standardized Uptake Value

**TBR:** Tissue-to-Blood Ratio

**TCP:** Tumor Control Probability

**TMR:** Tumor-to-Muscle Ratio

**VMAT:** Volumetric Modulated Arc Therapy

**WOV:** Well Oxygenated Volume

# Introduction

The potential damage that radiation can inflict to human tissues was discovered in the end of XIX century and few years later its application in medicine to defeat the spread of unhealthy cells in human body began. Along the decades the mechanisms of cells injury by radiation and of DNA repair were studied, leading to the application of the radiation doses fractionated in different sessions, as this generally results in a better sparing of the healthy cells surrounding the tumor [1].
The tumor microenvironment is fundamental for the understanding of its biochemical properties; in particular, among them the sensitivity of cells to radiation has a strong influence on the outcome of the treatment, with dependence on the stage of the cell life and on the level of oxygen carried by the surrounding vasculature. The second element is fundamental in Head and Neck Cancer (HNC), where a great part of the patients suffers of local tumor recurrence because of more radioresistant cells; indeed, it often happens that tumors in the head and neck have small volumes surviving in conditions of hypoxia, i.e. low levels of oxygen supply, connected normally to a lower cells death rate when exposed to radiation. The fractionation of the treatment in multiple doses provide one way to re-oxygenate the tumor in between fractions, thanks to the killing of the well oxygenated tumor cells surrounding the hypoxic ones: in this way the pressure due to the cell density decreases and the vessels can better oxygenate the region. But the fractionation of radiotherapy, despite allowing for re-oxygenation, normally it is not enough efficient when adopted alone; therefore other strategies, e.g. the exposition to hyperbaric oxygen or the assumption of radiosensitizers, have been envisaged, giving only discrete success [2].
In order to develop more efficient strategies it is fundamental to achieve better results in the field of hypoxia detection. From old standards methods, such as the polarographic $pO_2$ needle, to innovative ones, like magnetic resonance imaging coupled to reporter molecules like $^{19}F$, all of them present important cons, e.g. acquisitions limited by tumor accessibility, or lack of MRI systems implementing $^{19}F$ imaging in humans. But so far the most widely spread molecular imaging method is Positron Emission Tomography (PET), based on the detection of the radiation emitted by a radiotracer injected in the patient's body and retained by oxygen lacking cells. Nowadays, the most used radiotracer for the detection of hypoxia is $^{18}F$-fluoromisonidazole ($^{18}F$-FMISO), considered the gold standard for this purpose, while other tracers, possibly better in terms of image contrast, are still under investigation [3].
While there are many studies that analyzed the prognostic capacity of this tracer, only few articles tried to explain the mechanism of uptake, resulting in recent years in the development of a mathematical model able to explain it. Knowing the way with which FMISO is retained in macromolecules of hypoxic cells is of crucial importance for the improvement of the therapies. Indeed, the information provided by the tracer uptake itself could reflect the combination of multiple biochemical processes; if instead an uptake model is available, then the actual property of in-

terest (e.g. the oxygenation) could be imaged in a map.
The delivery of the dose is in the most of the cases given by an external source of radiation (external radiotherapy) and several techniques, such as volumetric modulated arc therapy and intensity-modulated radiotherapy, can sterilize the tumor volumes with high spatial accuracy. The implementation of dose boosting to the hypoxic subvolumes through the available technology, in the future could considerably improve the treatment outcome for patients affected by resistant tumors, avoiding the appearance of tumor relapses or metastases.
Even though the use of $^{18}$F-FMISO in PET imaging is not yet allowed for "dose painting" in radiation therapy, still it became acknowledged for its predictive power in prognoses of HNC and for proving the presence or the absence of re-oxygenation in the hypoxic regions.

The present thesis explored the conversion function defined by Toma-Dasu et al. [4] that maps the values of FMISO uptake into oxygen partial pressures, in a voxel-wise approach. In particular, the model requires as inputs a Well-Oxygenated Volume (WOV), taken as patient-specific reference, and its assigned $pO_2$ value: therefore, taken for granted the correctness of the model, the accuracy of the $pO_2$ maps obtained depends completely on the choice of the two mentioned parameters. Being the current study focused on HNC, the volumes acquired by PET imaging included only the head and neck regions; hence, the choice of the position of the oxygenated volume was limited to these portions of the body.
The second aim of this work was the improvement of the mathematical description of the re-oxygenation process happening after tumor irradiation. Starting from the oxygenation maps previously calculated, the histograms describing the distribution of $pO_2$ values in the neighborhood of the hypoxic volumes were generated for three different time points in the therapy; here the height of each bar represented the percentage of voxels within a specific range of $pO_2$. Subsequently, an evaluation of the best probability distribution fitting the mentioned data was done, associating a function, with the related parameters, to each histogram. Finally, the re-oxygenation process was mathematically characterized by the evolution in time of such functions.

Considering the application of the FMISO uptake model to real data, the target for the first problem is to test the similarity of the hypoxic volumes obtained with three different WOVs: the neck muscle, with oxygen partial pressure reference of 29 mmHg, the same with a value of 60 mmHg and a sphere in the shoulder region with $pO_2$ equal to 60 mmHg. The similarity has been evaluated not only between the volumes obtained with the mentioned model, but also between them and the current conventional method used nowadays for the same purpose, based on a threshold on the uptake values in the PET volumes. Indeed the choice of different WOVs influences the delineation of hypoxic subvolumes in shape, extension and localization, therefore it is necessary to compare the results possibly to the "ground truth"; being this information not available in practice, the target volumes were compared to the most studied method for their delineation, thresholding the

so called Tumor-to-Muscle Ratio in the PET images.
The second problem has been addressed with a technique that resumes the novel method presented by Lazzeroni et Al. in 2018 [5]. The functions describing the re-oxygenation process were obtained from the $pO_2$ distributions by solving a problem of deconvolution and exploiting the Fourier transform.

The thesis has the following structure:

- Section 1 will give a general introduction on the radiobiological aspects of the tumor microenvironment, indicating the various processes and factors in cells and tissues that can alter the effect of radiations in the human body; the effect of hypoxia on the radiosensitivity of the cells will be discussed more in detail, together with the process of re-oxygenation.

- Section 2 reviews the imaging techniques currently available for the spatial description of hypoxia in tumors, focusing in particular on PET imaging and all the existent radiotracers developed for their entrapment in hypoxic cells. Being the most studied and also the one used for this thesis, $^{18}$F-FMISO and its uptake process will receive particular attention.

- Section 3 describes the state of the art of the different techniques and machines currently adopted in the clinics for radiation therapies, along with the specific terminology adopted in RT for the definition of the targets. Also a review of the goals reached so far by FMISO in prognosis of the Head and Neck Cancers and of its expected future implementation in treatment plannings is presented, together with some comparison with other radiotracers for hypoxia. The last Subsection goes through the strategies that could be applied for the delineation of hypoxic volumes and for dose painting.

- Section 4 describes the material available for the study, with clinical details of the patients involved, and how the whole image dataset has been acquired; secondly, here the methods adopted for all the image analyses are presented, starting from the registration between different scanners to the $pO_2$ maps generated by using different WOVs and to the extrapolation of the parameters related to re-oxygenation.

- Section 5 presents the results obtained, with index of similarities for the volumes contoured with the methods described, and the graphical representation of the re-oxygenation functions.

- Sections 6 and 7 are left for the discussion of the results achieved and final conclusions are drawn.

# 1 Tumor microenvironment and hypoxia - general radiobiological aspects

A tumor is generally identified as an abnormal mass of body tissue that keeps growing relatively independently from the surrounding tissues, as tumor cells compete with healthy host cells for space and resources evading predation by the immune system.
The process that leads to the degeneration of this uncontrolled growth is related to variations in the normal life cycle of cells: old or damaged cells survive when they should die, while new cells form when they are not needed. Tumors can be distinguished in benign or malignant (cancerous) upon their aggressiveness towards healthy tissues: while the former have a metabolism similar to that of the host cells and thus do not grow fast, the latter invade nearby tissues and spread through te blood and lymph systems to other parts of the body often forming metastases [6,7].

Today one of the most applied therapies used for the treatment of tumors and cancers is the Radiation Therapy, which story began in 1895, when X-rays were discovered by W.C. Röntgen, and was later on developed with the discovery of radioactivity by Henry Becquerel and Marie and Pierre Curie [8]. The potential of radiation therapy in eradicating the tumors lies in the capacity of ionizing radiation to interact with cells, breaking the molecular bonds in DNA and thus preventing them from performing the normal activities and interactions with the healthy tissue. The effectiveness of the therapy depends on several factors: the particles and the energy of the rays, the fractionation scheme used, the repair time of sublethal damages, hypoxia are some of them.
Since nowadays the precision of machinery, both for imaging and for radiation therapy, are far away from achieving a cellular resolution, it is impossible to hit the whole mass of tumour sparing the surrounding healthy tissue; for this reason, to avoid unwanted damages and the generation of new tumors due to radiations, the tolerance of the latter has to be taken as reference for the therapy. There are numerous treatment schedules varying in time, delivered dose, number of fractions and depending on many agents, such as the localization of the tumor, its stage of spreading, the presence of hypoxic conditions, etc. In some cases it is suitable to deliver one single dose to the target, but often a fractionated treatment scheme leads to a better outcome for the patient; the choices made in the planning step must take their bases on the radiobiological aspects of the target and of the surrounding tissues.

First of all, it is important to consider the ways in which radiation induces damages that may lead to cells death and how the cells themselves try to repair such damages. The damage can be inflicted indirectly, when the ionizing radiation has an energy high enough to permit the break of chemical bonds between atoms or molecules and electrons, forming ions called Reactive Oxygen Species (ROS); in particular hydroxyl radicals, derived from water, are the biggest cause of DNA and

protein damages in RT. On the other hand radiation can break directly the DNA double-strand; even though this is a minor cause of DNA damage, the subsequent death of the cell is more likely to happen, especially in case of break of both the DNA strands [9].
Nevertheless, in case of Sub-Lethal Damages (SLD) the cell is able, in some measure, to counteract the loss of the DNA integrity going to repair (or better, to recover) the break in the strand due to the indirect or direct effect of radiation; the mechanism is only partially known, but *in vitro* and *in vivo* studies observed that the recovery generally occurs in few hours (up to 6 hours) after the irradiation [10]. Thus, although in this sense fractionated RT has a lower effect on tumor tissues, normal tissues suffer less complications concerning cells survival.
Another parameter is the Linear Energy Transfer (LET), defined as the energy transferred to the tissue by ionizing radiation per unit track length; high-LET radiations, condensing more energy in the same space, have more probabilities of directly hitting the DNA double-strand and so inflict lethal damages than low-LET radiations [11].
One of the main features to consider in RT is the cells radiosensitivity, defined as a measure of the response to irradiation with a given dose; it is often defined as the surviving fraction after receiving a dose of 2 Gy, where the surviving fraction is obtained *in vitro* as the ratio of the plating efficiency of treated cells to that of untreated control cells, where the plating efficiency is the percentage of seeded cells that grow into colonies. Radiosensitivity is influenced by numerous factors, among them being the tissue oxygenation probably the most relevant [12].
The particular condition in which the oxygen partial pressure in a specific tissue (usually the tumor) is low is called hypoxia and it is due to the presence of a poor vasculature and oxygen supply to the volume interested. Evidences show that hypoxic regions are less affected by radiation exposure and that the quantity of radiation needed to overcome this resistance with respect to normoxic tissues, the so-called Oxygen Enhancement Ratio (OER), reaches the value of about 3 in anoxic conditions [2]. Dose fractionation helps to re-oxygenate gradually the tumor, increasing its radiosensitivity [1].
Second, cells radiosensitivity is not constant, but varies along the life cycle; the most sensitive phase is M, when DNA is condensed and mechanisms of repair are lacking as well as life-cycle checkpoints, while the most radioresistant is the S phase [9]. According to the mechanism of redistribution, cells that are in a resistant phase during a fraction of treatment may progress in a more sensitive phase in the following fractions.
Last radiobiological feature to consider during the planning of a treatment with radiation is the phenomenon of repopulation: even after irradiation tumor and host cells keep on proliferating, leading to a sort of competition between the two populations. Repopulation of tumor cells is slow at the beginning of radiotherapy, but it speeds up after the first doses. This is called "accelerated repopulation" and begins after about three-four weeks of treatment for head and neck tumors. Accelerated repopulation becomes even faster if the treatment is interrupted after the tumor doubling time; for this reason it is preferable to postpone the start of the therapy

than interrupting it [11].

The study of the effect of ionization on cells is described in the commonly adopted survival curves, graphs representing the surviving fraction as function of the dose delivered. The most adopted model used to represent the survival curves nowadays is the Linear Quadratic (LQ) model [12], which relates the cell surviving fraction to the dose per fraction (assuming it as constant) and the number of fractions through the sum of two contributions: the first, proportional to the dose, is connected to lethal damages (cell deaths), and the second, proportional to the square of the dose, is due to sub-lethal damages, repairable within hours under normal conditions, unless an additional radiation dose is delivered.

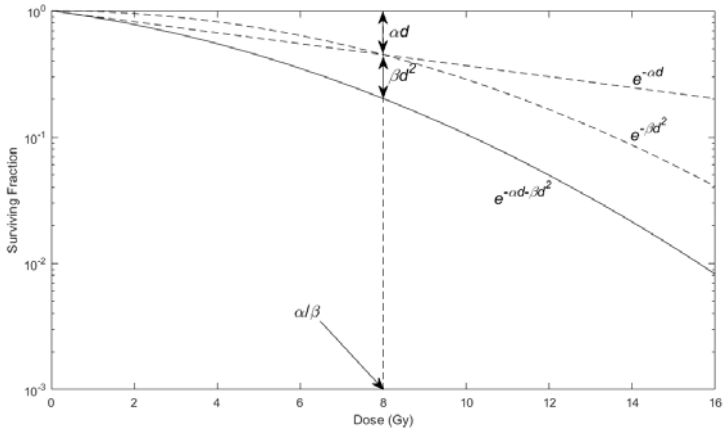


Figure 1.1: Surviving curve displaying the main parameters of the Linear Quadratic model.

The formula for multiple doses in oxic conditions results:

$$SF = [exp(-\alpha \cdot d - \beta \cdot d^2)]^n \tag{1}$$

where $SF$ is the fraction of surviving cells, $n$ is the number of fractions and $d$ is the dose per fraction, while $\alpha$ and $\beta$ express the proportion of the two contributions. In hypoxic conditions the above mentioned formula must be corrected by the OER, accounting for the higher resistance to ionizing radiation, as in the following:

$$SF = \left[exp\left(-\frac{\alpha \cdot d}{OER} - \frac{\beta \cdot d^2}{OER^2}\right)\right]^n \tag{2}$$

The ratio $\alpha/\beta$ is useful to describe the effect of fractionation and it is the dose for which the linear and quadratic components of cell death are equal, as visible in Fig. 1.1, and thus represents the level of curvature of the survival in the semi-logarithmic graph; that is, $\alpha/\beta$ expresses the sensitivity of the tissue under exam to fractionation [12]. Average values of $\alpha/\beta$ are 10 Gy for tumor response and early

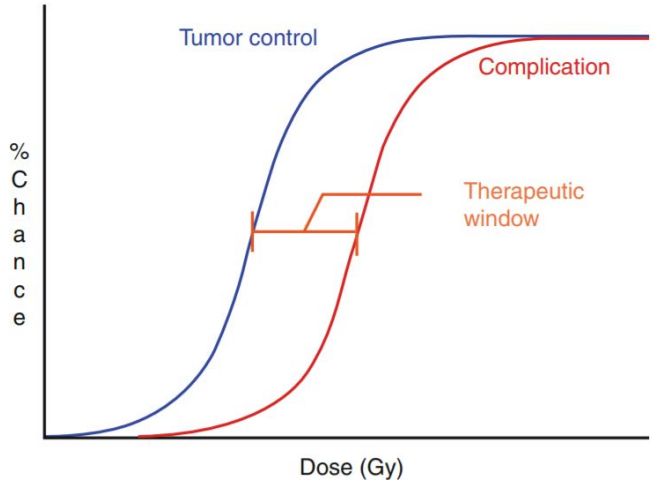


Figure 1.2: TCP (blue curve) and NTCP (red curve) as function of the delivered dose. Reproduced from "Basic Radiotherapy Physics and Biology" by Lasley, Foster D. et al. with permission of Springer International. Publishing in the format Thesis/Dissertation via Copyright Clearance Center.

responding tissues (here the response of the tissue comes earlier, without time for recovery of sub-lethal damages) and 3 Gy for late responding tissues [10].
Therefore hyperfractionation spares the tissues with low $\alpha/\beta$ (generally late reacting), while hypofractionation increases the effect of radiation in the same tissues.
Furthermore, in order to give an information about the effectiveness of the therapies, the concepts of Tumor Control Probabiity (TCP) and Normal Tissue Complication Probability (NTCP) have been developed. In order to achieve a successful treatment it is essential that the dose required to sterilize the tumor is lower than the minimum dose which may cause non-repairable damages in healthy surrounding tissues; the aim of radiotherapy is to maximize the therapeutic window, i.e. the distance between the two curves, because this would lead to safer and more effective therapies (Fig. 1.2) [13]. Both TCP and NTCP curves have sigmoid shapes; thus, the flatter and the closer to each other the two curves are, the more resistant to radiation the tumor is.
TCP increases with the dose and decreases with the number of cells in the tissue; the formula used to calculate it is:

$$TCP = e^{-SF \cdot N} \tag{3}$$

where N is the number of clonogenic cells in the tumor, i.e. proliferating cells.
The NTCP has a more complex expression, function of the total dose, fraction dose, fraction number, the volume of tissue exposed to the radiation and the presence of serial or portal organs [11].
As seen, the subject is wide, the factors involved in the outcome of RT are numer-

ous and complex, being the mechanisms of many of them only partially known. In the next subsections the focus will be on the oxygen effect on the radiobiology of cells and on how the problem of the increased radioresistance can be counteracted.

## 1.1 Hypoxia

The research in the field of tumor hypoxia has seen in the last decade a rapid growth in number of publications, since oxygen is one of the major key factors in determining the radiosensitivity of cells, and consequently the outcome of radiation and chemotherapy, especially in Head and Neck Cancers (HNC) [14].
While already at the beginning of the past century the effects of inadequate blood flow on X-ray imaging were seen, it was only after the half of the century that the possible consequences of hypoxia in radiation therapy were described for the first time, thanks to the advent of *in vitro* clonogenic assays. It was observed that necrosis in tumor clusters was present only if their diameter was higher than 0.4 mm, but what was more interesting to find was that, even if the size of the tumor mass increases, the thickness of the layer of viable cells remains constant at about 180 $\mu$m, corresponding roughly to the distance from a capillary at which the oxygen tension reaches 0 mmHg [15]. Hypoxic regions of tumors could be therefore sorts of shells of quite constant thickness and in which the oxygen tension is at a critical level, encompassing parts that are instead dead because of the complete lack of oxygen.
But the scenario is actually more complex: hypoxia can have origins connected to many parameters relative to blood vessels. A first distinction has to be made between *chronic* and *acute* (or *cycling*) *hypoxia*; their difference lies in the duration of the effects: while chronic hypoxia lasts from a few hours to many days, acute hypoxia resolves in less than 2 hours, usually with a quite constant periodicity [16]. More in detail, chronic hypoxia may be sub-categorized in [16]:

- *Diffusion-limited hypoxia.* Here the oxygen supply is limited by the distance to the tumor cells; the main reason for this is the absence of a robust vasculature near the tumor, where indeed cells started to spread irregularly and without giving the time to the surrounding capillaries to adequate their net of blood distribution and letting thus the oxygen to diffuse to all the cells in the tumor.

- *(Chronic) hypoxemic hypoxia.* Due to the constant reduction of oxygen content in the blood and/or a very high oxygen gradient along the vessels; the causes are related to anemia, functional anemia (heavy smokers decrease the availability of hemoglobin due to its binding with carbon monoxide) or oxygen supply coming from a vein.

- *Hypoxia due to compromised perfusion of leaky microvessels.* Being the microvessels in tumor areas dilated, tortuous and usually leaky, the gradient of

pressure between the arterial and venous ends decreases easily to 0 mmHg, because of the transmural coupling (in tumor tissues the interstitial fluid has higher pressure compared to the microvascular one).

When talking of acute hypoxia, it is possible to refer to [16]:

- *Ischemic hypoxia.* It is connected to a temporary block or a heavy reduction of the blood perfusion in a vessel, due e.g. to fibrin clots or masses of tumor cells obstructing its aperture, but also to vascular remodeling.
- *(Acute) hypoxemic hypoxia.* Transient and sharp reduction in the oxygen content in tumor microvessels, relative to temporary plasma flow or reduction in the number of red blood cells, besides possible common flow reversal in the capillary bed.

The consequences for each subtype of hypoxia are different in terms of perfusion, oxygen (and also nutrient) supply and waste removal, but they can be easily deduced by the above mentioned descriptions. Nowadays only few studies analyzed the biological and clinical effects of the two macro categories of hypoxia and they are often inconsistent; but what is generally found is the development of a more aggressive phenotype after acute hypoxia than after chronic hypoxia [17].
To give some reference numbers, hypoxic conditions are related to similar shapes in the survival curves, but the dose needed to reach a certain level of survival can reach 3 times the one needed in normoxic conditions and this value keeps constant at all levels of cell survival, making useful in this context to use a reference index as the OER [2].
The OER as function of the oxygen partial pressure has a fast growth till a tension of about 30 mmHg, then stabilizes at an almost constant level for all the following values of $pO_2$. Well-oxygenated tissues have oxygen partial pressure values of 30-70 mmHg [18], while the threshold for hypoxic ones is usually fixed at 10 mmHg, because this is the limit partial pressure at which some critic metabolic processes start to fail [19].

To overcome the problem of hypoxia, both acute and chronic, in radiation therapy five categories of aids have been explored in the last decades [20, 21]:

- **Increased oxygen delivery by the blood**
  - *Hyperbaric oxygen breathing.* It consists in the administration of oxygen under several atmospheres (generally 3) to the patient, with the aim of saturating the blood plasma and so extend the limits of the oxygen perfusion around capillaries, including in this way the hypoxic cells. Even though this technique gave better results in terms of tumor control in several clinical trials, it does not assure that the oxygen reaches the hypoxic regions; moreover it could give complications to other tissues, like some kinds of cartilage, which by nature have a low oxygen tension.

- *Normobaric oxygen/carbogen breathing and/or nicotinamide.* Carbogen with a mixture of 95% of oxygen and 5% of carbon dioxide at ambient pressure can reduce the level of chronic hypoxia in the tumor, while the joint administration of nicotinamide helps also the treatment of perfusion-limited hypoxia.
- *Blood transfusion.* Transfusions of blood with high concentrations of red blood cells in patients with hypoxic Head and Neck Squamous Cell Carcinoma (HNSCC) and low levels of hemoglobin have been tested in several clinical trials, however results did not demonstrate any significant improvement in the tumor oxygenation [22, 23].

- **Mimic of oxygen in the radiochemical process.**
  - *Radiosensitizers.* These molecules resulted to have similar, but weaker, effects to oxygen in the radiochemical process, reaching OERs of 1.5-2; in particular 5-nitroimidazoles and 2-nitroimidazoles have been the most studied radiosensitizers, while 2-nitroimidazoles utilization in the last decades moved towards the imaging sector of hypoxia. The limit of these compounds is their toxicity for the nervous system at the doses required. To date there is only one radiosensitizer, the nimorazole, used in HNC in the standard RT treatment.

- **Destruction of hypoxic cells.**
  - *Hypoxic cytotoxins.* Several selective cytotoxins towards hypoxic cells have been developed; nowadays it seems promising and worth of note a derivative of 2-nitroimidazoles, TH-302, currently in clinical development.
    Nitroimidazoles revealed themselves to produce cytotoxic metabolites specific towards hypoxic cells, but on a lower scale.
  - *Hyperthermia.* Pre-clinical studies showed that the heat can sensitize and eventually kill hypoxic cells when the tumor is contemporarily irradiated and taken to a temperature of 43°C; this is most probably related to the inhibition of DNA recovery.

- **Vascular targeting agents.**
  - *Angiogenesis inhibiting agents - vascular disrupting agents.* One way to prevent the formation of hypoxic tumors, but also tumors in general, is to counteract their growing vasculature. Angiogenesis inhibiting agents inhibit several steps in the angiogenic process, while vascular disrupting agents damage already existing tumor vessels. Despite their promising effects, it seems necessary to use them as coadjuvants in radiotherapy, because they do not increase the tumor control when used alone.

- **Radiation-based approaches.**

– *high-LET radiation.* The OER, besides to depend on the oxygen tension, is a quantity function also of the kind of radiation used: radiation with low-LET, $X$ or $\gamma$-rays for instance, present higher OER (from 2.5 to 3) than the ones with high-LET, such as $\alpha$-particles (close to 1); therefore the dependency on the oxygen tension is almost null for $\alpha$-particles [24]; here hypoxia passes in background in the treatment planning. Nevertheless, hypoxia can be completely ignored only when the LET value exceeds 500 keV/$\mu$m, a value not achievable clinically nowadays.

## 1.2 Re-oxygenation

The phenomenon of re-oxygenation appears when, after radiation exposure, most of the oxic tumoral cells die due to their higher radiosensitivity, while the surviving cells, mainly hypoxic, gradually achieve better vasculature and oxygenation and their radiosensitivity increases. In fractionated radiation therapy re-oxygenation happens through two modalities, connected to the two macrocategories of hypoxia described in the previous section [25]:

- *Slow re-oxygenation.* Connected to the diffusion-limited hypoxia, slow re-oxygenations happens when the ionizing radiations kill the more sensitive tumor cells near the capillaries, allowing a reduction of the interstial pressure and the revascularization of the area; as dead cells cannot consume oxygen anymore, hypoxic cells can reach higher oxygen tensions and reduce their radioresistance. This process is repeated fraction after fraction, helping to move the hypoxic layer towards the inner core of the tumor mass; the desired result is a small volume of well-oxygenated cells, more easily eradicable by the ionizing radiations (Fig. 1.3). The processes of slow re-oxygenation can last from some hours to several days.

- *Fast re-oxygenation.* In the context of acute hypoxia it is possible that the death of some irradiated cells obstructing the lumen of tumor microvessels can turn in their opening, restoring the blood flux within minutes to few hours; or the same effect may be due to a possible migration of few cell diameters. An important difference from the previous kind of re-oxygenation is the vitality of the hypoxic cells: while in slow re-oxygenation cells are starvating because of a chronic lack of oxygen, here cells are only temporarily deprived of it and can go on with their metabolic activities rapidly after recovering the supply; the consequence of this is an higher difficulty in the treatment of cyclic hypoxic cells when compared to the other because of the different sub-lethal damage repairing times.

However, despite its utility in achieving better treatment outcomes, the mechanism of tumor re-oxygenation nowadays is not yet fully understood and is matter of research.

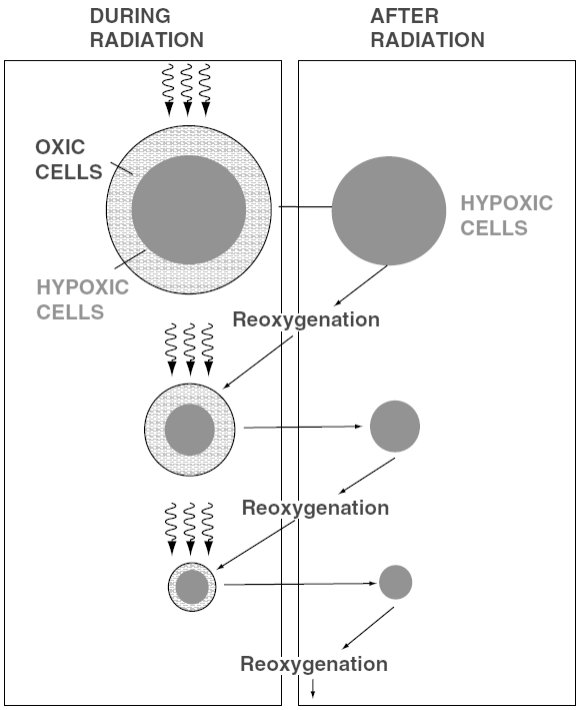


Figure 1.3: Fractionated radiotherapy and re-oxygenation. Reproduced from "Basic Radiation Oncology" by Beyzadeoglu, M. et al. with permission of Springer Nature. Publishing in the format Thesis/Dissertation via Copyright Clearance Center.

# 2 PET imaging of hypoxia

One of the major problems related to hypoxia since it began to be studied is its detection *in vivo*. Before the 1990s, effects of hypoxia were analyzed through radiation responses comparisons between the tumors of interest and tumors made anoxic in mice and rats; however this approach is qualitative and not suitable for the clinical practice, so researchers developed several techniques to quantify, directly or indirectly, the levels of $pO_2$ in tumors [2].

The polarographic $pO_2$ electrode (based on the $O_2$ Clark's electrode principle) has been considered for long time the gold standard for quantitative measure of tumor hypoxia; however, despite providing a direct measure of $pO_2$, it has a non-negligible effect on the actual levels of oxygen tension, only a specific part of the tissue $pO_2$ is represented and last, the procedure is particularly invasive and can damage the tissues [18]. After that, indirect measures of oxygen tension have been explored; particular signal sequences of Magnetic Resonance Imaging (MRI) paired with injected fluorocarbon reporters can give quantitative measure of hypoxia in tumors, however the limit of this procedure is the lack of human MRI systems supporting $^{19}F$ MRI. Blood Oxygenation Level Dependent (BOLD) MRI instead is a qualitative way to establish changes in the vasculature in tumors, although variations in signals are also connected to changes in oxy- and deoxy-hemoglobin concentrations, blood flow and vascular volume. Electron spin resonance, based on concepts similar to NMR, but imaged with spectrometers, has also been explored; its coupling with specific reporter molecules, such as char crystals or phthalocyanine, notably revealed sensitivity to oxygen content in tissues. However, the best results are given by direct injection of these compounds into tumor tissues, in order to avoid measurements biased by the uptake in the background tissues [3].

But probably the ideal way in which hypoxic cells could be detected would be one in which a molecular probe is not trapped when $O_2$ supply satisfies the demand of the cells and is instead retained when the oxygen supply is inadequate to permit the normal cellular respiration; moreover, since hypoxia is related to poor vasculature, it is important that this probe is delivered to all cells independently of the blood flow. Several molecules have been found to fulfill these requirements; in particular 2-nitroimidazoles, which at the beginning were used as radiosensitizers for hypoxic cells, demonstrated to give better results when labeled to image hypoxia through Positron Emission Tomography (PET) [3].

The late advent of PET in diagnosis and prognosis of tumors is due mainly to the delayed advances in the instrumentation technology with respect to those of synthetic chemistry, but now its sensitivity and versatility make it the most powerful molecular imaging technique for clinical use today available. Moreover its coupling with specific hypoxia tracers shifts its initial use from the detection of cancers to evaluation of their prognosis, with consequent selection of the most adapt treat-

(a)

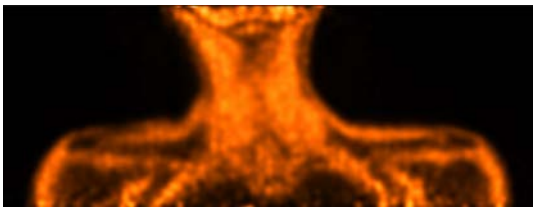

(b)

Figure 2.1: PET scanners produce functional images thanks to the radioactivity of injected radiotracers in the patient's vascular system. 2.1a shows a modern PET/CT scanner (the one also used for this thesis). Reprinted with permission from Philips. 2.1b represents a functional image obtained with the radiotracer $^{18}$F-FMISO, used for detection of tumor hypoxia.

ment for the specific patient. Fig. 2.1 shows a modern PET/CT scanner and a typical functional image obtained through the use of $^{18}$F-FMISO, a radiotracer adopted for the identification and delineation of tumor hypoxia.

PET machinery coupled also with Computer Tomography (CT) imaging can be adopted for different uses in oncology [26]: differentiation between malignant and benign tumors; primary tumor and metastases localization; grading malignancy, based on the concentration of tracer uptake; staging of cancer through full-body imaging; identification of residuals after the treatment; localizing eventual recurrences; measuring the effectiveness of the therapy adopted; guidance in radiation therapy, for radiation boosts in more radiosensitive areas of the tumor.

## 2.1 Radiotracers for hypoxia imaging

PET radiopharmaceuticals are generally classified upon their ability to image a specific biochemical process or on their process of localization in a specific organ or tissue of interest [27]. The development of radiotracers for hypoxia has focused almost only on 2-nitroimidazoles, as different studies showed that they act as oxygen

mimetics (even if their affinity is lower than the oxygen) and are trapped in cells that are hypoxic but still have electron-transport activity, i.e. hypoxic cells still alive, being the oxygen tension at a critical level, but not below 2-3 mmHg [28–30]. Before describing why 2-nitroimidazoles are so effective for the imaging of hypoxia (and what are their possible limits), it is worth discussing which are the main factors to consider before the development of a radiotracer [27]:

- *Size of the molecular imaging probe.* The dimension of the probe will determine how rapid is its clearance from nonspecific areas and from the blood circulation: the faster the washout, the higher will be the tumor to background ratio. This can be accomplished by smaller molecules; however it turns in lower specific activity, being restricted the possibility of binding more than one radiolabel per molecule.

- *Position of the radiolabel.* The localization of the radiolabel in the probe molecule must not influence its natural pharmacologic and chemical properties.

- *Lipophilicity.* The affinity towards lipophilic environments is highly dependent on the molecular mass, size and hydrogen-bonding capacity (polarity). This is an important parameter for the determination of the pharmacokinetics and dynamics properties of the radiolabel, such as the distribution in the tissues and its metabolism and elimination. It is generally calculated through an experiment involving the partition of the tracer between octanol and a buffer (commonly water).

- *Nonspecific binding.* The binding to proteins in blood plasma or to cell membranes are often occurrent, reducing in this way the amount of radiotracer available for the imaging of the target.

- *Specific activity.* It is the number of probe molecules capable of giving an useful radioactive signal for a given mass of radiotracer. It should be the highest possible, in order to prevent the saturation of the specific binding sites, with consequent decrease of contrast.

2-Nitroimidazoles are most commonly labeled with PET radionuclides such as $^{18}$F or $^{124}$I, but also $^{123}$I or even $^{99m}$Tc can be used. Anyway for the development of PET radiopharmaceuticals, $^{18}$F appears to be an ideal radionuclide; indeed, compared to other radiolabels, it takes several advantages, such as a relatively high specific activity, the possibility of production in high amounts, high resolution images (with a maximum of about 2.4 mm) and a half-lime time of 110 minutes, which is suitable for the transport from the cyclotron of production to the clinic [26]. For what concerns the probe molecules themselves, one strong advantage of 2-nitroimidazoles has been discovered in *in vitro* cultured cells and this becomes clear in Fig. 2.2: the range of oxygen partial pressures at which 2-nitroimidazoles are retained corresponds to the range at which OER varies steeply from about 3 in normoxic tissues to 1 in hypoxic ones, resulting in higher severity of hypoxia when

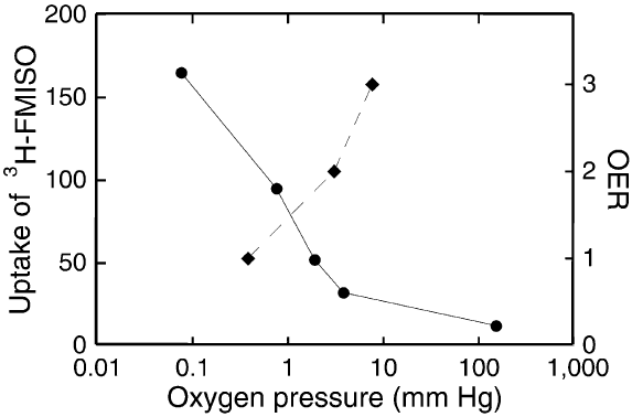


Figure 2.2: Uptake (arbitrary units) of $^{3}$H-FMISO (left axis and solid line) and oxygen enhancement ratio (right axis and dashed line) as function of oxygen pressure. Reprinted from "Molecular Imaging of Hypoxia" by Krohn, Kenneth M. et al. J Nucl Med. 2008; no. 49, pp. 129-148. © SNMMI.

the tracer uptake grows [3].
The radiotracers derivating from 2-nitroimidazoles currently studied for imaging of hypoxia are:

- $^{18}$F-FMISO, $^{18}$F-fluoromisonidazole;
- $^{18}$F-FETNIM, $^{18}$F-fluoroerythronitroimidazole;
- $^{18}$F-FETA, $^{18}$F-fluoroetanidazole;
- $^{18}$F-FAZA, $^{18}$F-fluoroazomycin-arabinofuranoside;
- $^{18}$F-HX4, $^{18}$F-flortanidazole.

Another tracer, belonging to another family of compounds, is matter of research for hypoxia:

- Cu-ATSM, Cu(II)-diacetyl-bis($N^4$-methylthiosemicarbazone)

In 1984, $^{18}$F-FMISO was proposed as a tracer for determining tumor hypoxia and nowadays is considered the gold standard for the assessment of hypoxia in PET imaging. So far it has been used to quantify tumor hypoxia in lung, brain, head-and-neck cancer patients and in the hearts of patients with myocardial ischemia.
The reason why $^{18}$F-FMISO is considered to be a good radiopharmaceutical prognostic for hypoxia lies in the fact that image pixels with a Tissue-to-Blood Ratio (TBR) equal or smaller than 1 are reliably normoxic. However, because of its dynamics in the human body (high lipophilicity, slow clearance kinetics, reaction

mechanisms and only passive transport), the identification and quantification of hypoxic tumor areas necessitate imaging for longer periods of time post injection [26].

$^{18}$F-FETNIM is more hydrophilic than $^{18}$F-FMISO and thus can be washed out more rapidly from well-oxygenated tissues compared to $^{18}$F-FMISO in preclinical studies and its synthesis is also simpler. In spite of the promising results, they need to be confirmed on a larger scale in order to be applied in the clinical practice [31].

$^{18}$F-FETA is more stable to non-hypoxic degradation *in vivo*, while its uptake reflects the $pO_2$ in the range 1-10 mmHg [3]; however it shows a less rapid metabolism by the body than $^{18}$F-FMISO [26] and further studies are needed to confirm its properties.

$^{18}$F-FAZA displayed a hypoxia-specific uptake mechanism and shows faster clearance than $^{18}$F-FMISO, providing high tumor-to-background ratios in less time [32]. Even its research is at a pre-clinical level and has not been adopted yet for tumor prognosis of patients.

$^{18}$F-HX4 is a novel radiopharmaceiutical derivated from 2-nitroimidazoles that showed reliable results in the definition of the hypoxic target, with faster washout times, higher contrast and sensitivity when compared to $^{18}$F-FMISO, even though only few studies have been conducted on human patients [33–35].

Cu(II)-ATSM instead plays a role in determining hypoxic regions through a mechanism of oxido-reduction, its uptake is more rapid than $^{18}$F-FMISO uptake, and the reported tumor-to-background ratio is about 3 times larger; despite this, the processes of uptake and clearance of the tracer are not yet completely understood [32].

## 2.2 $^{18}$F-FMISO biochemistry

The molecule of $^{18}$F-fluoromisonidazole (Fig. 2.3), despite the different structure from other 2-nitroimidazole analogs, has similar mechanism of trapping in hypoxic cells.

Nitroimidazoles enter cells by passive diffusion and, thanks to the affinity of the nitro group for electrons, undergo a single electron reduction (with the electron coming from the respiratory cycle of the cell) to form $-NO_2$, a potentially reactive radical anion, through the action of the enzyme nitroreductasi. When the oxygen concentration is high in the tissue, a molecule of $O_2$ accepts the electron from the anion, reoxidizing it. Instead, under hypoxic conditions, further reduction of the nitroimidazole occurs forming covalent bonds to intracellular macromolecules, leading to the entrapment of the probe in the hypoxic cell (Fig. 2.4) [3, 26]. Then

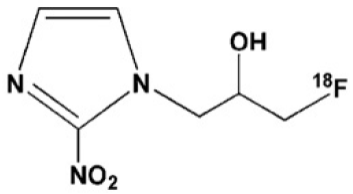


Figure 2.3: $^{18}$F-FMISO molecule. Adapted from "18F-Labeled Positron Emission Tomographic Radiopharmaceuticals in Oncology: An Overview of Radiochemistry and Mechanisms of Tumor Localization", no. 37, Vallabhajosula S., pp. 400-419, Copyright 2007, with permission from Elsevier.

the bound radiolabeled tracers can be visualized with PET imaging, giving information about the hypoxic volume of the tumor.

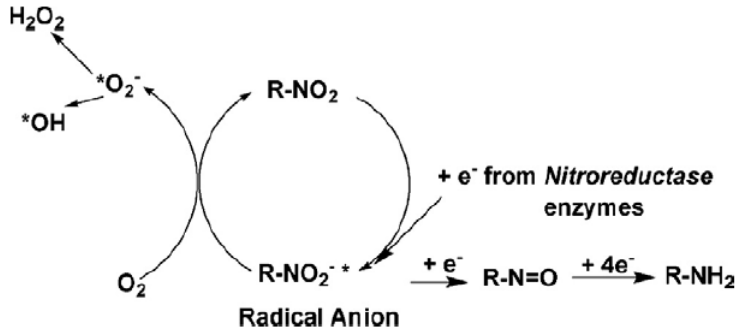


Figure 2.4: The mechanism of intracellular trapping of nitroimidazoles. Reprinted from "18F-Labeled Positron Emission Tomographic Radiopharmaceuticals in Oncology: An Overview of Radiochemistry and Mechanisms of Tumor Localization", no. 37, Vallabhajosula S., pp. 400-419, Copyright 2007, with permission from Elsevier.

The imaging protocol normally adopted for $^{18}$F-FMISO is quite simple, even though some differences in the timing issue are present among the different studies. When patients come to the clinic they are not required to fast before the study; the necessary dose of radiotracer (normally dependent on the weight of the patient) is injected and a static image acquisition starts from 90 to 120 minutes later with a duration of about 20 minutes, in order to collect a discrete number of emission events and get thus an higher contrast, even though lower compared to other radiotracers for hypoxia. Actually several studies showed that the contrast between the tumor and the background tends to increase (at least for 6 hours in rats, 4 hours in humans), without reaching a plateau in clinical useful time [36, 37]; for this reason the general trend in the last years is to adopt an interval of 4 hours post injec-

tion before the start of the static imaging. Normally during the imaging session a venous blood sample is drawn and the $^{18}$F-FMISO blood concentration is used to obtain a normalized map of Tumor-to-Blood Ratio (TBR) for each pixel in the image [3]. However in some cases this information could be missing, so it becomes necessary to use a reference region containing a well-oxygenated tissue; the choice of the reference is not univocal, because several factors, such as the position of the patient or partial body images, may interfere and lead to different results after the normalization; a common reference region for HNC is the posterior neck muscle and, instead of the TBR, a new parameter, the Tumor-to-Muscle Ratio (TMR) is adopted.
These maps are useful for the localization of hypoxic regions through the definition of a threshold on the TBR or TMR; Table 1 shows typical values reported in the literature concerning the TMR according to the protocol used. The values displayed could (in theory, if $^{18}$F-FMISO or other radiotracers will be validated for hypoxia imaging) be used for the treatment planning, considering an escalation of the dose accordingly to the levels of uptake [4, 36]. Despite the simplicity of directly using the uptake values, a map of $pO_2$ values would define more accurately the biophysical conditions and thus the treatment dose could be shaped according to the levels of oxygen tension, that generally are assumed to come from a nonlinear conversion function [4].
A novel sigmoidal conversion function based on the fitting of *in vitro* experimental data has been proposed in 2009 by Toma-Dasu et al. [4]:

$$pO_2(\mathbf{r}) = \frac{C \cdot (A - Uptake(\mathbf{r}))}{B + Uptake(\mathbf{r}) - A} \tag{4}$$

where $\mathbf{r}$ is the voxel in analysis, $A$ , $B$ and $C$ are reaction-specific parameters, which for $^{18}$F-FMISO result to be $A = 10.9$, $B = 10.7$, $C = 2.5$ mmHg [38]. More specifically the parameter $A$ is related to the reaction speed in the absence of the inhibitor and the second term (with parameters $B$ and $C$) describes the inhibition effect.
The $Uptake$ parameter in equation 4 is given by the uptake value in the voxel $\mathbf{r}$ in the FMISO PET, divided by the mean value in the selected Well-Oxygenated Volume (WOV) and multiplied by the tracer uptake obtained when equation 4 is applied using the reference $pO_2$ value for the WOV.

Table 1: Review on protocols and typical values of TMR in $^{18}$F-FMISO PET imaging

| **Type of tumor** | **Total number of pts** | **Age** | **Time of PET scanning** | **Start of PET scanning** | **FMISO dose injected** | **Muscle reference** | **FMISO SUVmax** | **FMISO TBR** | **FMISO TMR** | **TMR range** | **TMR threshold for hypoxia** |
|---|---|---|---|---|---|---|---|---|---|---|---|
| HNSCC | 17 | (median) 66 | Before treatment | 150 min p.i. | (median) 592 MBq | contralateral posterior cervical muscles | (median) 2.3 | | (median) 1.3 | | Median values (because of restricted dataset) [39] |
| OSCC | 22 | (median) 65 | Before surgery; 9 pts before chemotherapy, 13 pts after starting chemotherapy | 4h p.i. | 400 MBq | posterior cervical muscle | (median) 2.0 (range 1.3–3.5) | | (median) 1.5 | 0.99-2.96 | 1.25 [40] |
| OSCC | 23 (many from the previous study) | (median) 67 | Before treatment | 4h p.i. | 400 MBq | | | | (median) 1.4 | 0.9-2.1 | 1.25 [41] |
| HNC | 6 | | Before treatment | 4h p.i. | (median) 349 MBq | volume in neck muscle | | | (median) Primary: 1.8; Nodes: 1.2 | Primary: 1.5-3.8; Nodes: 1.0-3.4 | 1.4 [42] |
| HNC | 11 | (mean) 62 | Before treatment | 4h p.i. | (mean) 414 MBq | posterior cervical muscle | (mean SUV) 2.08±1.18 (range 1.21–5.01) | (mean) 2.98±0.72 (range 1.76-4.71; th. hypoxia: 1.5) | (mean) 2.23±0.67 | 1.22–3.82 | 1.25 [43] |
| HNC | 14 | (range) 46-70 | Before treatment | 4h p.i. | (range) 350–450 MBq | volume in neck muscle | (mean SUV) 2.54±0.81 | | (mean) 1.90±0.64 | 1.31-3.35 | [44] |
| NPC | 21 (9 with following local recurrence) | (median) 57 | Before IMRT | 4h p.i. | 400 MBq | posterior cervical muscles | | | (mean TMRmax) 1.86±0.17 (NR) and 1.94±0.18 (R) | | [45] |
| HNC | 72 | (mean) 60±11 (range) 25-86 | Before treatment | dynamic and static till 160 min p.i. | (mean) 390 MBq | contralateral neck muscles | | (mean) 1.35±0.31 (range 1.76-4.71) | | | 1.2 [46] |
| HNC, NSCLC | 26 (HNC) + 14 (NSCLC) | (median) 60.7 | Before treatment | 2h,4h p.i. | (range) 350–450 MBq | neck muscle (HNC), Mediastinum (NSCLC) | (range SUV) 1.1-4.3 (2h,4h,HNC), 1.2-2.7(2h,NSCLC), 1.0-3.7 (4h,NSCLC) | | (mean) 1.54±0.41 (2h,T/Mu,HNC), 1.72±0.52 (4h,T/Mu,HNC), 2.03±0.63 (2h,T/Me,NSCLC), 2.59±1.06 (4h,T/Me,NSCLC) | | 1.6 (T/Mu), 2.0 (T/Me) [47] |
| HNC | 20 | (mean) 55.8±11.4 | Before, during (30 Gy) and after IMRT | | 370 MBq | posterior cervical muscle | (mean) 2.58±0.97 (1), 1.74±0.44 (2), 1.56±0.35 (3) | | (mean) 1.84±0.49 (1), 1.30±0.24 (2), 1.13±0.12 (3) | | 1.25 [48] |
| HNSCC | 21 | | Before treatment | 4h p.i. | (mean) 371 MBq | neck muscle | | | | | 1.4 [49] |
| HNSCC | 15 | (median) 55 | Before treatment | 2,3,4h p.i | | Not defined | | | | | 1.4 [36] |
| HNC | 25 | | Before and during treatment | 4h p.i. | 250-300 MBq | deep neck muscle | (median and range) Baseline: 2.6 (1.9-4.3), after 8-10 Gy: 2.5 (1.7-4.3), after 18-20 Gy: 2.2 (1.0-3.8), after 51-57 Gy: 1.7 (0.3-2.4) | | (median) Baseline: 2.2, after 8-10 Gy: 2.2, after 18-20 Gy: 1.9, after 51-57 Gy: 1,7 | Baseline: (1.4-3.0), after 8-10 Gy: (2.0-3.9), after 18-20 Gy: (1.7-3.4), after 51-57 Gy: (1.5-2.2) | [50] |
| HNC | 24 | | Before treatment | 2h,3h p.i. | (mean) 314 MBq | ipsilateral nuchal muscles | (mean) After 2h: 1.0±0.1 (normoxic), 1.2±0.3 (hypoxic), after 3h: 1.2±0.4 (normoxic), 1.3±0.4 (hypoxic) | | (mean) After 2h: 1.4±0.1 (normoxic), 1.8±0.4 (hypoxic), after 3h: 1.5±0.4 (normoxic), 1.8±0.6 (hypoxic) | | [51] |

# 3 Head and Neck radiotherapy with external beams

Radiotherapy is a term coined in 1903 by Emil Grubbe, an American medical student who was most probably the first to apply radiation for clinical purposes [11]. Since then the field of radiation oncology spread and developed in the medical and scientific community. Its importance nowadays is underlined by the fact that more than 50% of cancers require radiotherapy, while about 25% may need a second radiation treatment due to recurrences [52, 53]. However in the clinical practice most of the cases are treated with a combination of different modalities, such as surgery, medical oncology, nuclear medicine and radiology.

Cancers are generally diagnosed basing on the stage of spreading (eventual metastases increase the severity of the pathology) and the area in which the primary tumor started to grow. In particular, Head and Neck Cancers are the ones involved in this study; about 630.000 patients are diagnosed of HNC cancer every year in the world, while the death incidence is over 55%, involving especially Head and Neck Squamous Cell Carcinomas (HNSCC). Many are the reasons that can promote the development of HNC: they can arise because of bad habits (smoking and alcohol are the most correlated to HNSCC; use of dry snuff, particularly adopted in Sweden and USA, is highly correlated to Oral Squamous Cell Carcinoma (OSCC)); viral infections, such as papilloma virus (HPV) ia another possible cause of HNC; genetic tendency plays a role as well; even the exposure to radiation (for instance previous radiotherapy) and to sun may be cause of skin carcinoma; other possible risk factors are vitamin deficiencis, poor oral hygiene, chronic infections and prostheses characterized by low biocompatibility with human tissues [11, 54].

Independently on the location of the cancer, the kinds of radiation therapy can be distinguished upon the aim: it may be curative, especially when the cancer volume is limited and localized in a specific site; palliative, for instance in case of metastases, in order to alleviate the symptoms; preventive, when the aim is to prevent possible metastases or recurrences; total body irradiation, for suppression of the immune system when the bone marrow needs to be transplanted. It is opportune to specify in this context that in the head and neck region the lymphatic network is particularly rich of vessels and each site-specific cancer has its specific route for lymph node metastasis [11].

## 3.1 Generalities on type of external beam radiotherapy

According to the location of the radiation source, radiotherapy may be classified in [11]:

- *External radiotherapy (teletherapy/external beam radiotherapy).* Radiotherapy applied to the body externally using a treatment machine.

- *Brachytherapy (endocurietherapy/sealed-source radiotherapy).* Radiotherapy based on placement of permanent radiation sources in body cavities.

- *Intraoperative radiotherapy.* Kind of radiotherapy delivered usually through low-LET beams immediately after the surgical resection of the primary tumor.

As this study focuses on external beam radiotherapy, it is necessary to have a general look on the different techniques and machines nowadays adopted for cancer treatment with the radiation dose being delivered from outside the body. They are [11, 55–57]:

- *Image-Guided RadioTherapy (IGRT).* It involves coregistered anatomical (CT, MRI and ultrasounds) and functional (fMRI, PET) imaging techniques to increase the precision of the therapy, accounting for variations in volume and shape of the target during the treatment and adapting to them. It can be included in other techniques.

- *Stereotactic Body RadioTherapy (SBRT).* Radiotherapy delivered by several beams based on a 3D model of the target volume. The requisites of this technique are: secure patient immobilization through customized molds for the body; accurate tumor relocalization with the assistance of IGRT techniques; a system solving the problem of movements due to respiration (in case of liver and lung tumors), e.g. X-ray tumor tracking. It is different from Stereotactic RadioSurgery (SRS), most adopted for brain recurrences or metastases, while SBRT is applied to lung and lymph node cancers and lung, spine, bony metastases. The main benefit of these approaches is the reduction of the length of the therapy (hypofractionation) through the delivery of higher doses, sparing in a better way the normal tissues than conventional RT.

- *Three-Dimensional Conformal RadioTherapy (3D-CRT).* A technique by which the dose volume is made to conform closely to the tumor volume through the use of 3D anatomical data coming from CT or MRI imaging. Recent 4D-CRT treatment plannings include in the analysis also the breathing movement, designed especially for treatment of non-small cell lung cancer (NSCLC).

- *Intensity-Modulated RadioTherapy (IMRT).* An evoluted form of 3D-CRT, according to which the dose distribution that conforms to the target is composed by non-uniform beam intensities, permitting a more effective sparing of normal tissues and local dose boosts to less radiosensitive volumes (especially when IGRT is supported).

- *Tomotherapy.* A particular IMRT technique consisting in the delivery of the dose in slices in a serial or helicoidal mode.

- *Volumetric Modulated Arc Therapy (VMAT).* A novel radiation technique based on the simultaneous variation of three parameters during the dose delivery: the gantry rotation speed, the shape and aperture of the beam and dose rate.

- *CyberKnife®.* A kind of SBRT/SRS technique in which a linear accelerator mounted on a robotic arm with 6 degrees of freedom delivers the dose volume from numerous points in space (nodes, normally 100-200) spherically distributed around the patient. The possibility of mounting a linear accelerator (linac) on a robotic arm is due to the smaller dimensions with respect to normal linacs; indeed this machine works in the X-band (wavelength: 2.5-3.75 cm) instead of the normal adopted S-band (wavelength: 7.5-15 cm). Accurate detection of target motion and tracking of the radiation beams are ensured by a pair of stereoscopic in-room X-ray tubes and associated flat panel detectors; although the imaging is in 2D, and not 3D given by Cone-Beam CT (CBCT) as in many other units, this gives an advantage in terms of speed of detection, processing and corrections of the robotic manipulator. Moreover the recent addition of multi-leaves collimator to the assembly lets the modulation of the dose giving an IMRT/SBRT combined modality.

- *Gamma Knife Icon (GKI).* Kind of SBRT machine capable of managing more than 10 isocenters for the treatment of complex tumors thanks to the presence of 192 radiation sources positioned in a CT round shape. A CBCT imaging unit is integrated and aligned with the radiation unit for online correction of the treatment.

Furthermore, even a number of different types of radiation beams are used for radiotherapy. These include X-rays, electrons and other particles like neutrons, protons, negative pi-mesons, as well as heavier nuclei such as carbon, helium, neon, and silicon ions.
When planning the treatment essentially three types of volumes need to be defined by the medical team [58, 59]:

- *Gross Tumor Volume (GTV).* Macroscopic contouring of the most cell dense malignant growth to determine its localization and extension; it is based on anatomical and/or functional images, palpation or visual analysis (when superficial). It includes the primary tumor and eventually lymph nodes or other metastases.

- *Clinical Target Volume (CTV).* It includes the GTV and a margin accounting for spreads of the tumor cells into nearby tissues; here the tumor cell density is lower, nevertheless this region needs to receive a certain dose if the aim is a curative therapy, as in this case only the eradication of all the tumor cells leads to a successful RT treatment.

- *Planning Target Volume (PTV).* It encompasses the CTV and is related to the precision of the machinery used for the imaging and the treatment. It is defined by the Systematic Target Volume (STV) plus a random error margin: while the former accounts for errors in treatment preparation, the latter considers all the possible accuracy errors that may arise during the treatment execution.

- *Internal Target Volumes (ITV).* It is a volume, generally asymmetric around the CTV, that takes into account its variations in position, shape and size, due for instance to movements connected to respiration or heart beat.

In some cases it is useful to delineate the Planning organ at Risk Volumes (PRVs), which are volumes surrounding Organs At Risk (OARs), i.e. tissues or organs that need absolutely to be spared in favor of the avoidance of crucial side effects; an example of such organs is the spinal cord.
And to conclude, an important volume when talking of hypoxia is the Hypoxic Target Volume (HTV).

## 3.2 The role of FMISO in Head and Neck Cancer imaging

Although nowadays $^{18}$F-FMISO is the most used radiotracer for the detection of hypoxia, at the current state it has not reached the level of acknowledged drug applicable in the oncological clinical practice, as conversely $^{18}$F-fluorodeoxyglucose ($^{18}$F-FDG) did for the enhancement of tumor metabolism in PET imaging.
Therefore it is useful to resume where the research has lead and what has confirmed so far, in order to better understand what are the directions to pursuit for a further validation and for the introduction of $^{18}$F-FMISO in the clinical use, at least for what concerns head and neck cancers.
So far the studies carried out on the radiotracer related to HNC seem to agree on the following aspects:

- The fractionation of the total dose in multiple consecutive delivery steps leads to the re-oxygenation of the tumor, especially at the beginning of the treatment (usually first 20 Gy / 10 fractions) [48, 60, 61].

- Different parameters, such as the maximum Standardized Uptake Value (SUVmax), TBRmax, the TMR, hypoxic volumes, especially at the first-second week of treatment, are factors that could predict the prognosis of the disease in radiotherapy and radiochemotherapy. They have proven to discriminate reliably between responders, for which the standard RT is suitable to eradicate the cancer, and non-responders, i.e. patients showing high correlation to further recurrences due to high level of hypoxia [39, 47, 50, 61–64]. The same consideration applies for FMISO PET images of HNC patients acquired before chemotherapy alone [40]. This point will be discussed in detail in Subsection 3.3.

These results are confirmed by statistical significance, however they can provide methods only for the assessment of the biological responsiveness of a patient in terms of speed of re-oxygenation of the tumor and possible outcome of the therapy. They do not give straight answers to questions like "Is $^{18}$F-FMISO a reliable radiotracer? / Are the obtained images reproducible?", "How do the hypoxic volumes evolve in shape and localization during time?" and "Is it effectively possible to counteract hypoxia in HNC with the use of RT? And if yes, how?". The answers to these topics have been examined by different groups of research, but did not conclude with definitive verdicts, due especially to the small size of the patients cohorts involved in these clinical trials.
While the third question will be discussed in detail in Subsection 3.4, here the attention is put on the first two.

The reproducibility of $^{18}$F-FMISO has been tested on different cohorts of HNC patients. A study of 2013 involving 11 HNC patients tested the repeatability of the results comparing the values of SUVmax, TBR, TMR and hypoxic volumes between two PET scans acquired with the same protocol 48 hours apart, achieving high correlations (>90%) between the pairs of parameters [43]. A previous work revealed a high correlation (71%) in uptake in a GTV voxel-by-voxel analysis between pairs of PET pre-treatment images acquired 3 days apart for 20 HNC patients; however this decreased to 46% when only the presumed hypoxic volumes were considered [65], indicating the possibility of the presence of a bias term (chronic stable hypoxia) and a fluctuating component (acute or cyclic hypoxia). But two problems here arise: the hypoxic volumes were delineated with a threshold on the TBR, yet so far any study showed the stability of radioactivity in the blood; moreover, the acquisitions were made in temporal ranges of minutes too wide (117-195 min, and 126-195 min respectively for FMISO 1 and FMISO 2) for a reliable analysis (see section 2.2) [66]. There is also in literature the proposal of a model for tissue oxygenation and FMISO dynamics that includes the contributions of chronic and acute hypoxia separately [67]: here the high prevalence of chronic hypoxia to the cyclic one in the cause of retention of FMISO in hypoxic volumes is proven (87% vs 13%); it is also observed that, even varying the timepoint of the tracer injection along all the acutely hypoxic cycle, the variability in FMISO uptake is not significative.

For what concerns the dynamic and morphology of hypoxia, a few studies showed that the hypoxic subvolumes have different patterns of shape change during the treatment (completely resolved, decreasing stable, decreasing unstable, increasing hypoxia); the overall tendency in the majority of patients is a decrease in volume with a rather stable localization [68,69]; another study reports a geographical miss of 20% between repeated $^{18}$F-FMISO PET images during the treatment in HNC [70], most probably due to unpredictable changes in tumor vasculature at a cellular level.

## 3.3 Investigating the tumor response to radiotherapy in Head and Neck Cancer patients with hypoxia tracers

The predictive value of PET imaging in Head and Neck Cancer is still matter of study for all the hypoxia radiopharmaceuticals; however, so far $^{18}$F-FMISO confirmed in many more studies than for other tracers its capability of categorizing the patients between RT responders and non-responders.

Among the other radiopharmaceuticals for detection of hypoxia, only $^{18}$F-FAZA has been tested by more groups for predictive purposes.
One of the most relevant work is the one carried out by Mortensen et al., who examined data coming from 40 HNC patients undergoing RT or radiochemotherapy; the hypoxic volumes where defined by a threshold of 1.4 on the TMR and 9 out 10 recurrences happened in patients defined as hypoxic, while the remaining patient was considered non-hypoxic with a borderline TMR of 1.3 and did not complete the therapy [71].
Similarly, Saga et al. proved, by a FAZA imaging analysis for 23 HNSCC patients undergoing radiochemotherapy, that the TMR pre-therapy is the only prognostic factor for determination of progression-free survival (p-value=0.01) [72].

For pre-RT $^{18}$F-FMISO imaging, one of the first and most important results, because of the number of patients involved (N=73), reveals as the strongest factor associated to patient survival the TBRmax, followed by the HTV, in an univariate analysis of pre-treatment PET images [62].
In another early study involving 15 HNC patients, the univariate analysis detected a weak statistical significance (p-value close to 0.05) for the SUVmax and no significance for the hypoxic fraction; here the negative prognosis was linked to tumor recurrence, instead of the patient decease [73].
An analysis carried out by Kikuchi et al. on 30 HNSCC patients found high correlations with treatment outcome (presence or absence of relapses) in SUVmax and TMR parameters (p-values 0.02 and 0.04 respectively) [39].
Eschmann et al., by analyzing the clinical course of 13 HNC patients, found predictive power (presence of relapses) in SUV with images acquired 4 hours post injection (p-value=0.04), but not for the same factor 2 hours post injection (p-value=0.16); also a threshold of 1.6 on TMR 4 hours p.i. allowed to perfectly discriminate between responders and non-responders [47].
To conclude this sequence of pre-radiotherapy image analyses it is noteworthy the phase II clinical trial developed by Welz et al., which revealed that the branch of 10 HNSCC patients receiving counter-hypoxic dose escalation presented better outcomes in terms of local tumor control with respect to the branch of 10 patients receiving the standard radiotherapy (70.0% vs 44.4%). In this case a baseline dynamic FMISO PET-CT was used to generate a value of malignancy for each voxel depending on hypoxia and tumor perfusion; the HTV was determined by a threshold on the coefficient of malignancy [63].

Repeated $^{18}$F-FMISO imaging for HNC prognosis was carried out by three groups. Zips et al. enrolled 25 HNC patients, imaged once before and three times during radiochemotherapy; they demonstrate that in an univariate analysis, the most powerful predictive parameters for local recurrences are the TMR and the SUVmax at the second week of treatment (p-values of 0.008 and 0.015, hazard ratios of 4.25 and 3.85, respectively) [50].
Wiedenmann et al. obtained similar results; in fact, they analyzed 16 HNC patients in three time points before and during radiochemotherapy, finding the best correlation between presence of tumor recurrences and TMR during the second week of treatment (p-value=0.016) [61].
Similar results, coming from a pooled cohort of 50 HNC patients undergoing radiochemotherapy, are given by the work of Löck et al. They indicate that the prognosis can be reliably determined by the hypoxic volume before the treatment, at week 1 and 2 (p-values of 0.008, 0.01 and 0.008) and by the TMR at week 2 (p-value=0.017) [64].

Recently, a novel approach conducted by Lazzeroni et al. proposed a new method for revealing in a systematic way the predictive power of FMISO. The process consists in the temporal evaluation of the distribution of $pO_2$ values in the hypoxic volumes; indeed, often multiple FMISO imaging sessions are taken before and during the therapy and today it is also possible to convert the uptake into oxygen tension maps [4]. The objective is to determine how the tumor re-oxygenates during the course of RT, by looking at how the histograms representing the oxygen tension distributions evolve in time (normally three time points are considered: one before and two during the therapy). Looking in detail the algorithm, initially the histograms of the hypoxic volumes are fitted with a log-normal distribution, obtaining three functions ($f_1$, $f_2$ and $f_3$) characterized by the relative parameters; they can be seen as the known inputs and outputs of two blocks representing the re-oxygenation processes (unknown), described by the functions (or impulse responses, using a term of the systems theory) $g_1$ and $g_2$. Therefore, $g_1$ convolves with the oxygen tension distribution at the first time point ($f_1$) to give the second ($f_2$), while $g_2$ convolves with the second distribution ($f_2$) to give the third ($f_3$). The process of convolution can easily be substituted by the application of the Fourier transform and anti-transform, replacing the convolutions with the products [5]. More details on the methods are given in Subsection 4.4.2.
The application of this method on a big cohort of patients could lead to the classification of different patterns of tumor re-oxygenation, with the possibility of predicting the prognosis of the disease after the treatment by looking at the parameters of the re-oxygenation function.

## 3.4 Possible dose escalation strategies exploiting FMISO imaging

To date the treatment plans in RT do not use the information provided by functional imaging of hypoxia; nevertheless, several groups tested the feasibility of incorporation of radiosensitivity parameters connected to hypoxia in the so-called "dose painting", i.e. the delivery of higher doses to the hypoxic volumes to counteract tumor cells with low $pO_2$ [74].
The dose painting techniques developed so far can be subdivided into two groups [74]:

- *Dose Painting by Contours (DPBC).* This method is usually based on the use of a fixed lower threshold, e.g. on the TBR or TMR, to define the hypoxic subvolumes; generally this permits an easier software implementation and the production of an uniform dose boost prescribed to the hypoxic subvolume. Chang et al., for instance, evaluated the use of a protocol for HNC, where the hypoxic target is delineated by a TMR $\geq 1.5$ and the correspondent PTV receives a dose of 84 Gy, when in the standard treatment the maximum dose delivered to the PTV is of 70 Gy [75]. Choi et al. instead explored the delivery from 2.6 to 3.6 Gy more per fraction with respect to standard treatment to hypoxic targets defined by a tumor-to-cerebellum ratio of 1.3 [76].

- *Dose Painting by Numbers (DPBN).* While DPBC works generally on properties of the full patient volume, such as the histogram of uptake values, this approach is voxel-based. The dose to deliver to each voxel is calculated and planned by the use of biological parameters, such as the $pO_2$ level or the growth rate of cells in some cases; these maps can be obtained by simple models, relating the uptake to the correspondent parameter in a linear way, or by more complex and better describing representations, such as exponential or sigmoidal models [4, 38].

The research by now has spent more energy on DPBC; different single-center works tested by simulation the feasibility of dose painting for IMRT and VMAT, obtaining in general a considerable increase in TCP and stability or a small increase in NTCP when a pre-treatment $^{18}$F-FMISO image is acquired [75–78]; this is proved also by the fact that loco-regional recurrences in HNC arise mainly from hypoxic subvolumes in the primary GTV [79]. Similar results have been obtained for a phantom simulation with $^{60}$Cu-ATSM [80] and repeated $^{18}$F-FAZA PET images [81]. But, although the high correlation between FMISO uptake and tumor control, the patterns of re-oxygenation are pretty variable during the therapy, with the necessity of utmost care during the planning and the use of multiple imaging during the treatment [75, 77, 78, 81, 82]. Thus an adaptation of the treatment along the different sessions is generally needed for hypoxic patients [70]. By now there are also doubts concerning the threshold to use on TMR (see Table 1): a study of Henriques de Figueiredo et Al. based on pretreatment FMISO PET images demonstrated that

the static threshold method gives double hypoxic volumes when compared to an adaptive threshold or to a stochastic method, indicating that probably a fixed threshold is too conservative, as it could include parts of the tumors with levels of $pO_2$ higher than 10 mmHg, that could be misleading [36].

The DPBN branch has been concentrating on the power and significativity of biological features: indeed the relationships between tracer retention and $pO_2$ values are not linear and the model supporting the oxygen transport to tumor capillary beds is complex; if we add to this the fact that what we can image with PET are voxels having a resolution on the order of the mm, while the oxygen transport to tissues happens on the $\mu$m scale, then a model connecting the two domains is required [74].
Different paths based on different PET imaging modalities have been examined.
The first is founded on specific doubts about the use of static PET images, because they lack of an important parameter characteristic of each tumor microenvironment: the perfusion efficiency; the combination of the perfusion in the tumor microenvironment with the tracer uptake would reveal specific patient information, with a consequent categorization of the patient tumor re-oxygenation and thus the possibility of a specific tailored therapy [73]. This can be obtained from dynamic PET images, for which different models have been developed [83, 84]; simulations gave also better results when compared to uniform dose boosts in terms of TCP [85]; nevertheless, this analysis is not yet feasible in the clinical practice because of more complex imaging protocols.
An alternative solution exploiting the relative higher simplicity of static uptake maps is the use of an oxygen transport model that can connect directly the tracer uptake domain to the oxygen partial pressure domain; a possible non-linear conversion function had already been presented in Subsection 2.2. In the same paper of Toma-Dasu et al. describing the sigmoidal uptake model, three treatment approaches for hypoxia have been advanced and compared to the standard radiation treatment. The first method adopts the tumor radiosensitivity at a pre-clinical level, considering hypoxia as a stable phenomenon throughout the time; a dose-modifying factor associated to the Linear Quadratic model is therefore used to deliver a dose boost to the hypoxic subvolumes. The second approach takes into account variations in tumor oxygenation over time, by including in the planning FMISO images acquired even during the treatment. The last involves a segmentation of the tumor volume in CTV, GTV and HTV, and an escalation of the standard dose to each segment inversely proportional to the steepness of the correspondent dose-response curve; this results in an effective dose to the whole tumor volume, as the model simulation confirmed, giving the best results in terms of tumor coverage and tumor control. Despite its clinical utility, the third method requires more technical resources and would be therefore suitable for patients presenting extensive tumor hypoxia; indeed the second method demonstrated only a fewer tumor coverage achieving the same TCP, and thus, being also less resources demanding, would be more appropriate when patients present not extensive or even absent hypoxia [38].

It remains anyway fundamental to investigate precisely how the hypoxia patches evolve during the course of the treatment and what are the contribution of cyclic and chronic hypoxia in FMISO PET imaging.

# 4 Materials and methods

## 4.1 Patients

In this study, between 2014 and 2017 thirty HNSSC patients enrolled for a clinical trial and have been treated with radiotherapy in the Universitätsklinikum of Freiburg with a total dose of 70 Gy fractionated in five fractions of 2 Gy per week; for each patient two or three clinical target volumes, shown in Fig. 4.1 for one representative patient, were defined:

- HN1, the volume receiving 50 Gy of dose, and
- HN2, boost volume within HN1, receiving further 10 Gy of dose + HN3, boost volume within HN2, receiving further 10 Gy of dose, or
- HN2, boost volume within HN1, receiving 20 Gy of further dose.

Figure 4.1: Clinical Target Volumes indicated by the medical team for dose delivery in the tumor volume. HN1 is marked with blue, HN2 with red, while HN3 with green color.

Also, concurrently with RT, chemotherapy with three cycles of cisplatin 100 mg/kg/d (or carboplatin in case of chronic renal insufficiency) were administered. At the date of diagnosis the median age was 60 years, with a range of 34-77 years; the median follow-up time was 21.54 months, with a range of 1.51-49.28 months. 6 patients deceased during the experiment due to local recurrences or other circumstances, while in total 14 patients presented recurrences during the follow-up period.
The patients' imaging procedure consisted of an initial planning CT before the treatment (12.07 $\pm$ 3.52 days, range 5-22 days), of one co-registered $^{18}$F-FDG PET-CT before the treatment (8.59 $\pm$ 5.95 days, range 0-31 days) for a better tumor

delineation and to three co-registered $^{18}$F-FMISO PET-CT at different imaging stages: the first before the treatment (5.65 ± 2.66 days, range (-2)-8 days); the second after a mean dose of 16.03 ± 4.56 Gy (11.10 ± 3.92 days after the beginning of the treatment; range 6-23 days); the third after an overall mean dose of 46.30 ± 5.67 Gy (33.03 ± 5.34 days after the beginning of the treatment; range 27-51 days). Fig. 4.2 introduces an example of the available set of images for one representative patient.
In Table 2 the main characteristics of the patients and the timing of the FMISO imaging are reported.

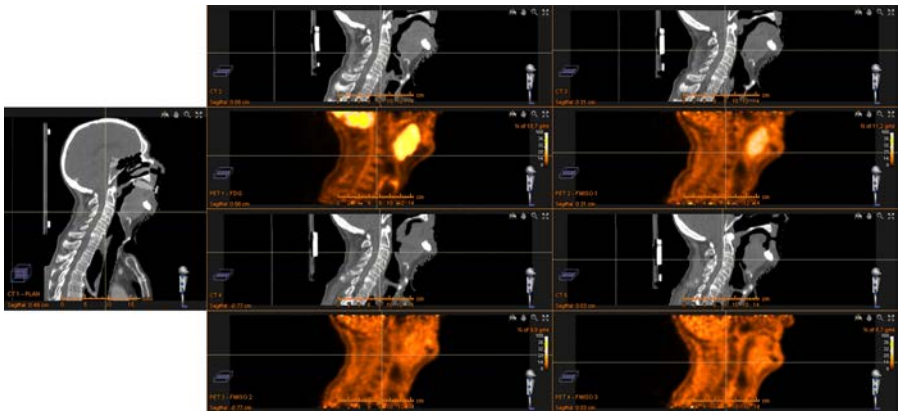

Figure 4.2: Sample of available images (Patient 22): planning CT on the left; CT-FDG PET pair on the high left corner; CT-FMISO PET 1 on the high right corner; CT-FMISO PET 2 on the low left corner; CT-FMISO PET 3 on the low right corner.

## 4.2 Protocol of PET-CT image acquisition

The patients were not required to fast before the imaging sessions. The CT/PET scanner adopted comes from Philips brand, the specific model being GEMINI TF Big Bore. The position of the patients was the same used for the radiotherapy treatment, while the static imaging process started 167 ± 15 minutes after the injection of 302 ± 17 MBq of $^{18}$F-FMISO and lasted 20 minutes.

## 4.3 Image registration in RayStation

The analysis conducted on the three pairs of PET-CT images acquired for each patient before and during the treatment has been possible thanks to an hybrid De-

Table 2: Patients' characteristics

| No. | Age | Follow-up time (months) | Time to loco-regional recurrence (months) | Time to decease (months) | Delivered dose at $2^{nd}$ FMISO PET (Gy) | Delivered dose at $3^{rd}$ FMISO PET (Gy) |
|---|---|---|---|---|---|---|
| 1 | 60 | 36.92 | | | N.A. | N.A. |
| 2 | 52 | 24.33 | 16.79 | 24.33 | N.A. | N.A. |
| 3 | 53 | 12.13 | 5.18 | 12.13 | 20 | 56 |
| 4 | 51 | 25.77 | | | 14 | 44 |
| 5 | 61 | 28.85 | 6.95 | | 12 | 42 |
| 6 | 54 | 23.41 | 10.36 | | 22 | 40 |
| 7 | 66 | 15.15 | 5.18 | | 26 | 50 |
| 8 | 51 | 19.48 | 14.56 | | 12 | 40 |
| 9 | 60 | 11.18 | | | 20 | 44 |
| 10 | 70 | 11.54 | | | 12 | 42 |
| 11 | 56 | 8.56 | | | 14 | 44 |
| 12 | 60 | 3.61 | | | 12 | 40 |
| 13 | 60 | 48.23 | | | 12 | 52 |
| 14 | 49 | 43.34 | | | 20 | 46 |
| 15 | 60 | 44.30 | 8.16 | | 20 | 48 |
| 16 | 63 | 43.08 | 12.82 | | 16 | 54 |
| 17 | 63 | 36.75 | N.A. | 36.75 | | 40 |
| 18 | 41 | 34.23 | 6.66 | 34.23 | 18 | 46 |
| 19 | 54 | 8.95 | | 8.95 | 20 | 50 |
| 20 | 77 | 36.95 | | | 20 | 59 |
| 21 | 69 | 16.03 | 10.52 | | 14 | 41.13 |
| 22 | 34 | 1.51 | | | 24 | 54 |
| 23 | 67 | 15.74 | | 15.74 | 12 | 40 |
| 24 | 42 | 24.79 | 7.05 | | 20 | 52 |
| 25 | 60 | 5.97 | | | 8 | 38 |
| 26 | 67 | 21.54 | | | 12 | 50 |
| 27 | 57 | 19.34 | 9.70 | | 12 | |
| 28 | 57 | 10.72 | 7.80 | | 12 | 54 |
| 29 | 67 | 8.62 | | | 14 | 46 |
| 30 | 65 | 3.02 | | | 14 | 46 |

formable Image Registration (DIR) implemented in a research version of RayStation [86]. This technique has been recently introduced for HNC; although its spatial accuracy has proven to be high, further validation of the algorithm is required [87]. The algorithm at the base of hybrid DIR in RayStation is called ANACONDA, standing for "ANAtomically CONstrained Deformation Algorithm", which com-

bines intensity information with anatomical information given by contoured image sets, with the purpose of avoiding as much as possible the smoothing of images containing only intensity information and keep the whole anatomical information [86]. Algorithms involving only the first approach try to match the image intensities voxel-wise or patch-wise, loosing the guarantees on the reliability of the anatomical matching, especially in low-contrast regions; the second group instead uses hundreds of landmarks pointed by the specialist on meaningful and evident structures, which are then registered to the target image and used to derive a deformation vector field: the drawback in this case is a reduction in accuracy where landmarks are less dense. The objective (non-linear) function maximized adopted by ANACONDA is the weighted sum of [86, 87]:

- an image similarity term (e.g. a correlation coefficient), based on a combination of image intensities and geometrical structures; in this way only the benefits coming from the two approaches are achieved, while the drawbacks are avoided.
- a grid regularization term, to keep the image grid smooth and invertible;
- a penalty term, when controlling structures (such as the patient contour) are present.

Each patient was registered following two separated steps: first, a rigid registration based on the bony anatomy; second, a deformable registration based on the previous algorithm.
The process of registration (rigid transformation + hybrid DIR) for each patient and each pair of PET-CT volumes consisted in the registration of the low dose CT (the one acquired concomitantly with the correspondent PET) to the planning high dose CT, while the application of the latter transformation to the PET scan was implicit, as they belong to the same frame of reference.
This method lets every pair of CT-PET volumes to be co-registered and finally registered to the reference planning CT. Fig. 4.3 gives a schematic representation of the registration process and Fig. 4.4 shows an example of coregistered images.

## 4.4 Methodology

### 4.4.1 Analysis of the influence of the reference region

Once the registration procedure is completed, a set of superimposable anatomical and functional images for each patient is available for further analyses.
The following step is the application of the model described in Subsection 2.2 in order to obtain maps of oxygen partial pressure, by using equation 4. Particular attention should be put on the choice of the Well-Oxygenated Volumes, together

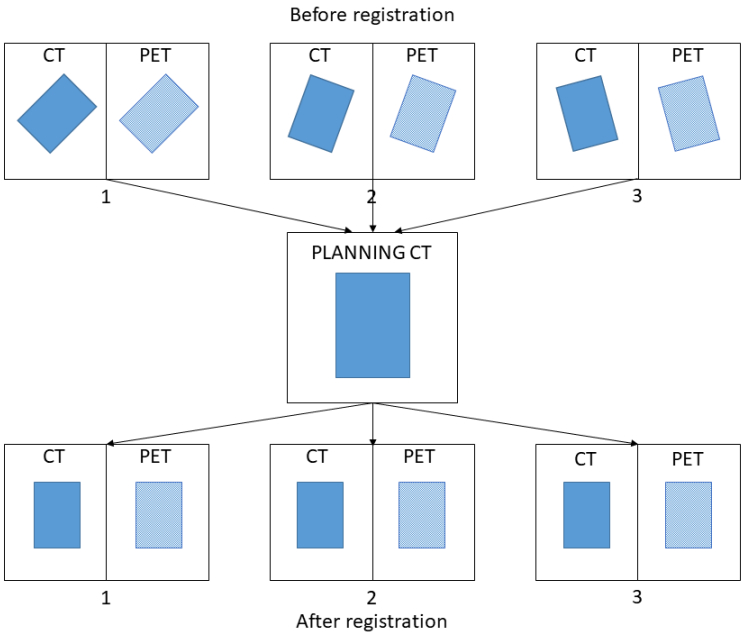


Figure 4.3: Representation of the registration process: at the beginning, the CT-PET coupled images are inherently registered; what follows is the hybrid deformable registration of the low-dose CT to the planning CT; the same transformation takes automatically place in the PET images, because they belong to the same frame of reference of the corresponding CT images. As a result, all the CT-PET pairs are registered with the planning CT and between themselves.

with their reference values.
Several WOVs have been tested, but some of them were discarded before further considerations. Indeed two first attempts were the cerebellum and the ear lobe; the problems found with them were the absence of cerebellum in many of the CT-PET acquisitions and the inconstancy of the position of the ear lobe after the hybrid deformable registration, due to the small size of the ROI located at the border of the patient's anatomy. Hence two kinds of reference region were considered: the posterior deep neck muscle and the shoulder muscle; it was not possible to extend the choice of the reference to other regions, since the PET volumes included a narrow band of the body focused on the tumor volume; in fact, as Fig. 4.4 displays, in most of the patients the visible parts were the inferior part of the head, the neck and part of the shoulders.
For all the patients but 9 the neck region was already delineated by a medical doctor, while for the others a box with dimensions 5x4x2 $cm^3$ was manually drawn and considered as a surrogate of the neck delineation. For all the patients a sphere of radius 1.25 cm (volume 1.95 $cm^3$) was generated in the shoulder muscle in a

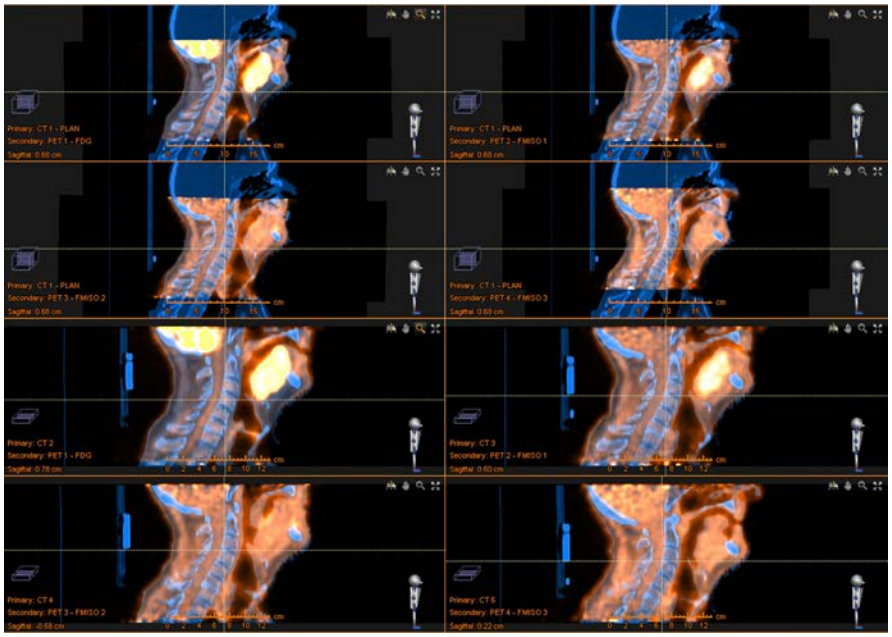

Figure 4.4: Example of hybrid registration (Patient 22). From top to bottom, left to right: planning CT overlapped with PET FDG, PET FMISO 1, PET FMISO 2, PET FMISO 3; CT-PET FDG; CT-PET FMISO 1; CT-PET FMISO 2; CT-PET FMISO 3, respectively.

region of low CT density. Fig. 4.5 reports an example of such regions.

The three FMISO PET images were then converted into oxygen tension maps through the non-linear model presented in section 2.2. The research version of RayStation implements a module called Functional Analysis that permits to apply the sigmoidal model to the data and export them if necessary for further analyses with other softwares. With the parameters values for A, B and C defined previously three maps have been generated for each FMISO PET image, corresponding to the three following WOVs:

- neck muscle, with reference value 29 mmHg;
- neck muscle, with reference value 60 mmHg;
- shoulder muscle, with reference value 60 mmHg.

The last two reference values come from values adopted in the original model [38], while the first has been chosen because a work of Carreau et al averaged different studies, finding 29.2±1.8 mmHg as $pO_2$ value for skeletal muscles [18].
For each map the HTV inside HN2 (one of the CTVs) was defined through the

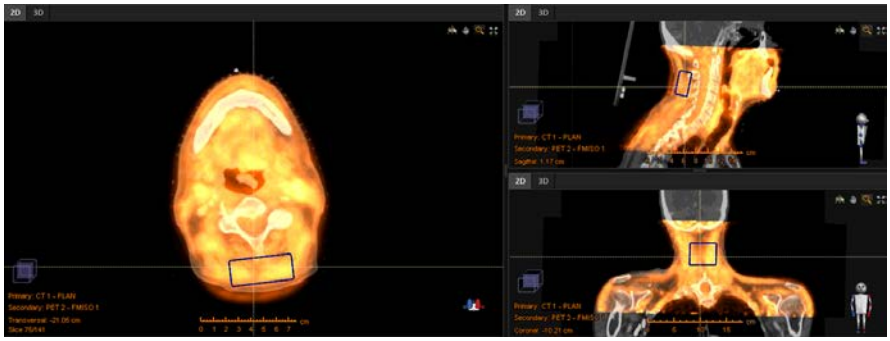

(a)

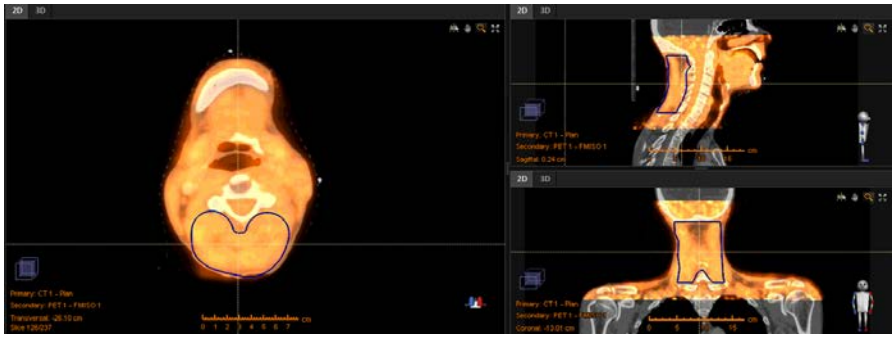

(b)

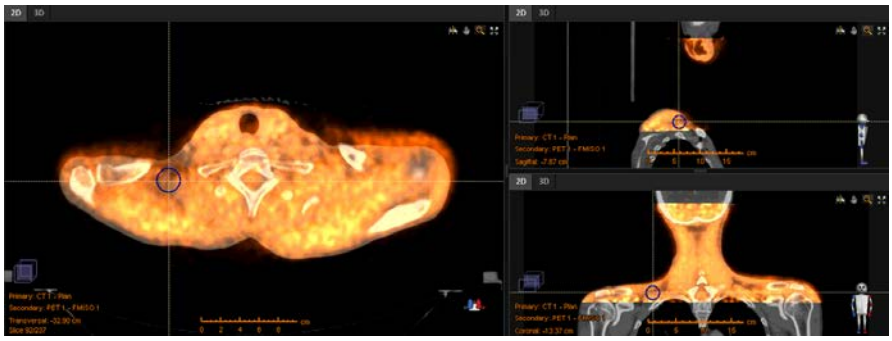

(c)

Figure 4.5: Examples of adopted WOVs (FMISO PET 1 coregistered images are superimposed to the planning CTs): 4.5a. Patient 23, neck box; 4.5b. Patient 11, manually drawn neck region; 4.5c. Patient 11, sphere in the shoulder region.

standard threshold of 10 mmHg. In order to compare this work with the others in the topic (see Subsection 2.2), the hypoxic volumes have been defined also in the FMISO PET images, choosing 1.4 as lower threshold for the TMR and the neck

muscle as reference; indeed, as Table 1 displays, this is the most common practice. The quantification of the similarity between the pairs of volumes derived from the conversion functions and the standard method using TMR $\geq 1.4$ has been done by using the DICE coefficient. The DICE coefficient for two volumes, $DICE(V_1, V_2)$, is defined as the ratio between their intersection, $V_1 \cap V_2$, over their union, $V_1 \cup V_2$. Another element evaluated is the correlation between the curves representing the trend of hypoxic volumes during the therapy. This was accomplished by calculating the normalized cross-correlation coefficient with zero lag between signals, i.e. for the two signals $x$ and $y$ the normalized cross-correlation coefficient is $R_{xy}(0) = \frac{\sum_{n=1}^{3} x_n \cdot y_n}{\sqrt{\sum_{n=1}^{3} x_n \cdot x_n \cdot \sum_{n=1}^{3} y_n \cdot y_n}}$; here, 0 is the maximum shift between the signals, while 3 is the number of time points corresponding to FMISO PET images.

### 4.4.2 Modeling parameters of re-oxygenation

The aim of this part of the study was to establish first of all the best distribution fitting the histograms of $pO_2$ values in the HTVs, and, after this, to find a pattern of re-oxygenation functions connecting the fitted distributions among the three different time points.
The theory behind this is quite simple. Considering the three oxygen tension maps, it is possible to represent the values of $pO_2$ by histograms. Let us suppose that their shape is fitted by three functions, $f_1$, $f_2$ and $f_3$; then we can imagine this like a system (see Fig. 4.6), where the impulse response, $reox$, characterizes the re-oxygenation process. By the systems theory, the output is given by the convolution of the impulse response with the input; moreover, from the Convolution Theorem the operation becomes the product of the Fourier transforms of the input and of impulse response. In formulas, considering for instance the first block, $F_2 = REOX \cdot F_1$, where $F_2 = \mathcal{F}\{f_2\}$, $REOX = \mathcal{F}\{reox\}$ and $F_1 = \mathcal{F}\{f_1\}$. A final Fourier anti-Transform of the found $REOX$ furnishes the desired re-oxygenation function $reox$: $reox = \mathcal{F}^{-1}\{REOX\}$.

Since the choice of the posterior neck muscle corresponds to the same region adopted in the standard method, while the reference value of 29 mmHg is granted by the literature, this analysis has been conducted only for the maps coming from this latter case.
Therefore the following procedure has been followed for each patient:

1. From the $pO_2$ map derived from the first FMISO PET, the HTV inside the HN2 has been selected.

2. The selected region has been expanded 1 cm in each direction, in order to consider the HTV with the surrounding tumor environment.

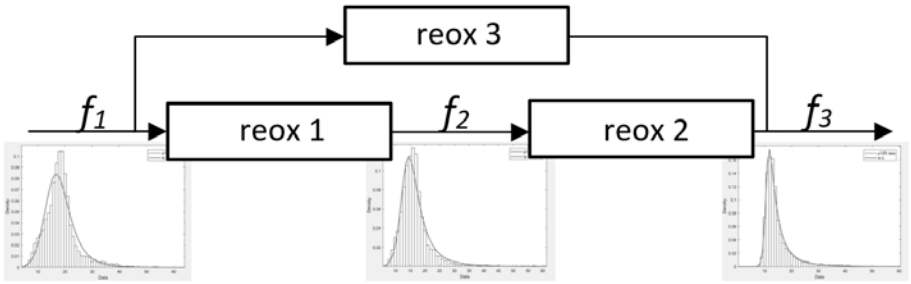


Figure 4.6: Schematic representation of the re-oxygenation system among the three time points in the therapy.

3. The expanded region has been intersected with the HN2, as by definition it is not expected to have tumor cells outside the CTV.
4. The region obtained has been copied in the second and third maps derived respectively from the second and the third FMISO PET image of the patient.
5. The three maps of $pO_2$ values have been exported to generate the histograms to fit through Matlab v. 2017b and Origin v. 2018b.
6. Different distributions have been evaluated for the fitting of the histograms and the ones with the best fitting were kept for further comparisons; in this way the functions $f_1$, $f_2$ and $f_3$ were generated. Also the influence of the binning of the data with different widths and different methods was evaluated.
7. The functions $f_1$, $f_2$ and $f_3$ were shifted into the frequency domain applying the Fourier Transform, obtaining $F_1$, $F_2$ and $F_3$.
8. The re-oxygenation functions $REOX1$ (mapping $F_1$ to $F_2$), $REOX2$ (mapping $F_2$ to $F_3$) and $REOX3$ (mapping $F_1$ to $F_3$) were calculated.
9. The inverse Fourier Transform provided the desired re-oxygenation functions in the initial domain, $reox_1$, $reox_2$ and $reox_3$.

In particular for the point 6 the concentration has been posed on the LogNormal distribution and on the Burr distribution; the former is given by the following density:

$$f(x) = \frac{1}{x\sqrt{2\pi}} \cdot exp[-\frac{(ln(x)-\mu)^2}{2\sigma^2}], \tag{5}$$

where $\mu$ and $\sigma$ are respectively the mean and the standard deviation of the distribution; the Burr density instead is given by:

$$f(x;c,k,\lambda) = \frac{ck}{\lambda} \cdot \frac{x^{c-1}}{\lambda} \cdot [1+\frac{x}{\lambda}^{c}]^{-k-1}, \tag{6}$$

where $c$, $k$ and $\lambda$ are three parameters.

# 5 Results

In this Section, the results obtained will be presented structured in two parts. The first part shows how the choice of the WOV can affect the contouring of the hypoxic subvolumes. The second one deals with the mathematical characterization of the re-oxygenation curves.

## 5.1 On the selection of the well oxygenated reference region

The $pO_2$ maps generated by using the different WOVs returned results characterized in general by rather considerable differences in terms of extension of hypoxic volumes and localization. In the following an example of images obtained for a representative slice of Patient 9 is displayed; it is also possible to see the evolution of hypoxia estimated by the three methods based on the conversion model and by the standard method based on DPBC (Fig. 5.1-5.3 and Fig. 5.4, respectively). The oxygen tension maps given by Fig. 5.1 show the change in location and size during treatment of the hypoxic region in the tumor when using as WOV the deep neck muscle with a reference value of 29 mmHg; in this case, the initial volume almost disappeared already after the second week of treatment. In Fig. 5.2, instead, the map of $pO_2$ values never displays values below the threshold of 10 mmHg; this was found in all the patients but 2 when using the WOV corresponding to the posterior deep neck muscle with a reference value of 60 mmHg. The case of Fig. 5.3, where the WOV adopted is the sphere in the shoulder region with 60 mmHg as reference, is different from the previous two: here, indeed, the volume found is large already before the treatment and keeps staying high, with a slight decrease, until the fifth week of treatment. Finally, Fig. 5.4 shows the standard method based on the threshold of 1.4 on the Tumor-to-Muscle Ratio, giving hypoxic volumes definitely larger in all the FMISO PETs than the three conversion maps.
It is of interest to compare the minimum value of $pO_2$ inside the hypoxic targets, the hypoxic volumes and the similarity between pairs of volumes. The first two are displayed in Fig. 5.5 for each FMISO PET and each patient, while the similarity is further on discussed in this Subsection.
As reasonably expected, the general trend for the minimum level of $pO_2$ is a slight increase during the treatment, as tumor re-oxygenation takes place; at the same time the hypoxic volume decreases in most of the patients.
As already described, the use of the posterior neck muscle as WOV with 60 mmHg of oxygenation reference leads to an unlikely result, i.e. only Patients 1 and 20 resulted hypoxic before the treatment and after that any trace of hypoxia is found. Conversely, the HTV given by the conventional method for this dataset is always non-zero for all the patients, with rather high values for every PET imaging; this is also an improbable case, as generally for HNC studies the percentage of hypoxic patients decreases considerably during the treatment, while this dataset does not

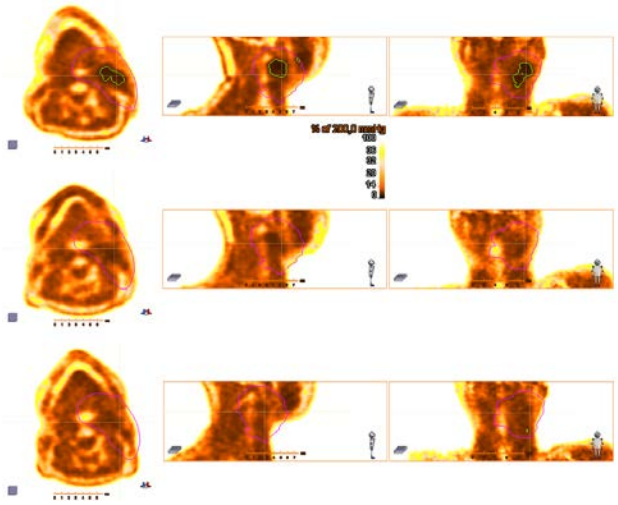

Figure 5.1: Example of $pO_2$ maps generated by using as WOV the posterior deep neck muscle with 29 mmHg as assigned oxygenation level. Every row is related to the correspondent FMISO PET (1, 2 and 3); HN2 (magenta) and HTVs (green) are delineated.

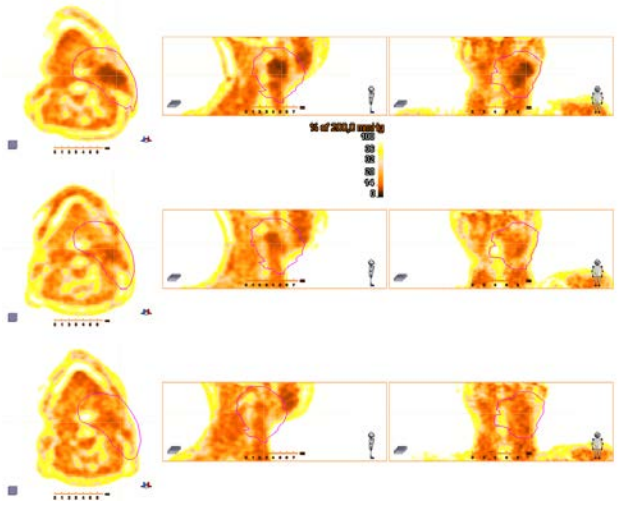

Figure 5.2: Example of $pO_2$ maps generated by using as WOV the posterior deep neck muscle with 60 mmHg as assigned oxygenation level. Every row is related to the correspondent FMISO PET (1, 2 and 3); HN2 (magenta) and HTVs (green) are delineated.

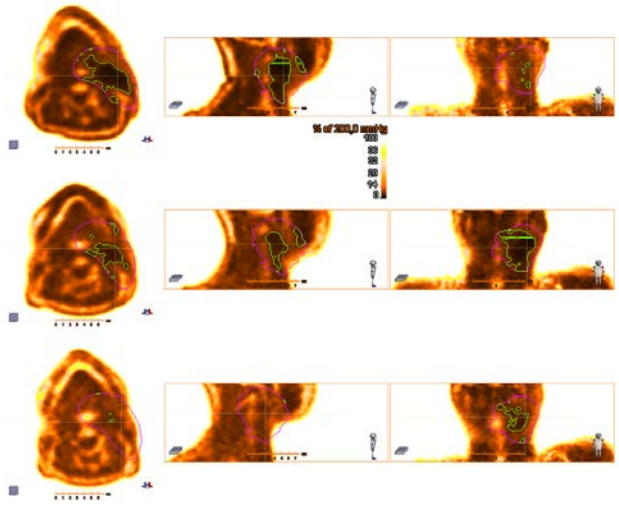

Figure 5.3: Example of $pO_2$ maps generated by using as WOV a sphere in the shoulder region with 60 mmHg assigned oxygenation level. Every row is related to the correspondent FMISO PET (1, 2 and 3); HN2 (magenta) and HTVs (green) are delineated. Sagittal frame in FMISO 1 and coronal frame in FMISO 2 present an artifact connected to software visualization.

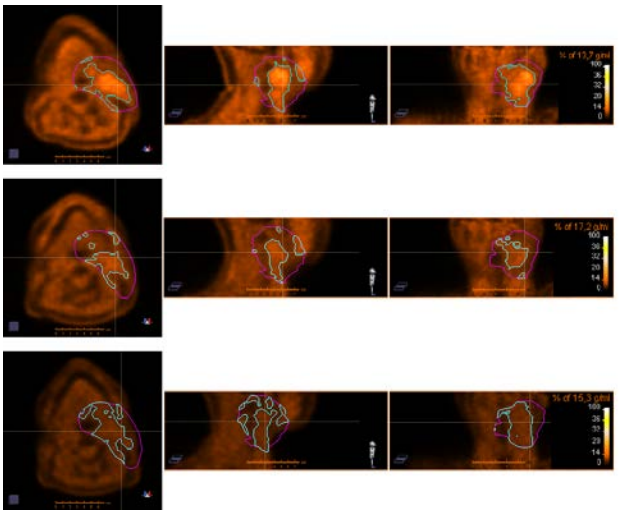

Figure 5.4: Hypoxic volumes determined on the FMISO PET images with the standard method (TMR $\geq$ 1.4). Every row is related to the correspondent FMISO PET (1, 2 and 3); HN2 (magenta) and HTVs (light blue) are delineated.

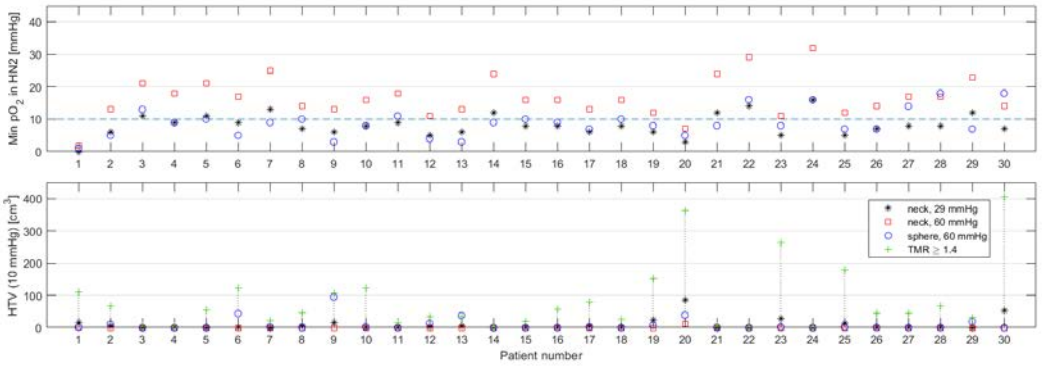


(a)

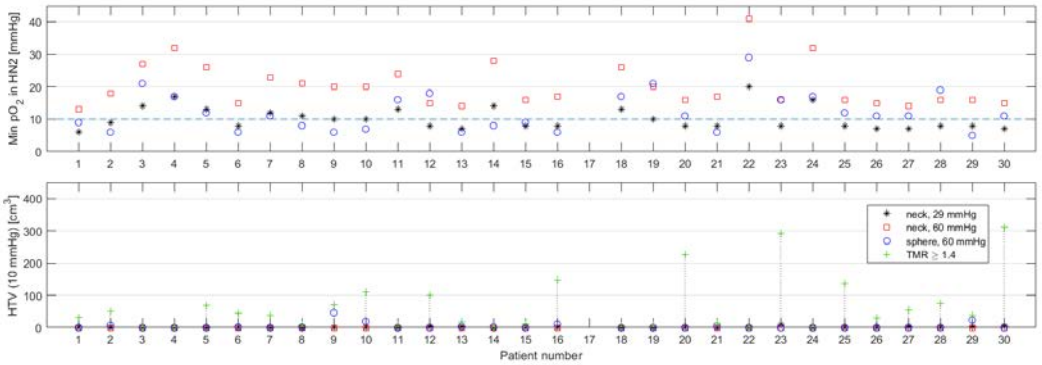


(b)

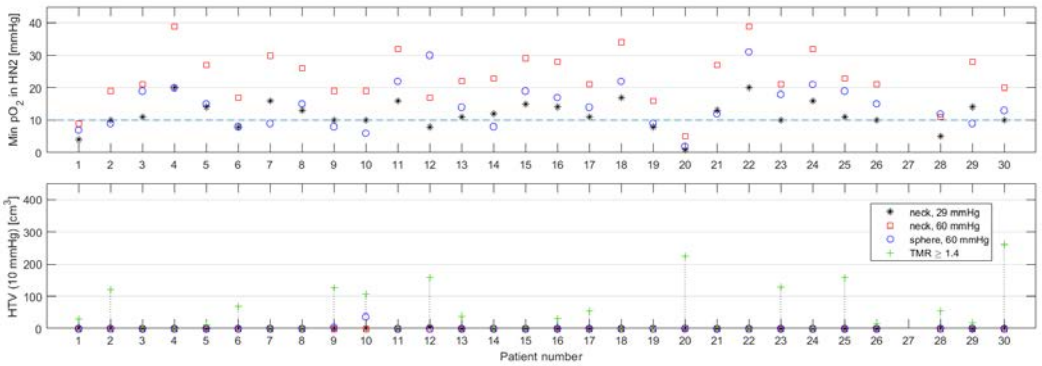


(c)

Figure 5.5: Plots of the minimum $pO_2$ values in the hypoxic targets resulting from the uptake model application and of the hypoxic volumes found with the four different methods for FMISO PET 1 (5.5a), 2 (5.5b) and 3 (5.5c).

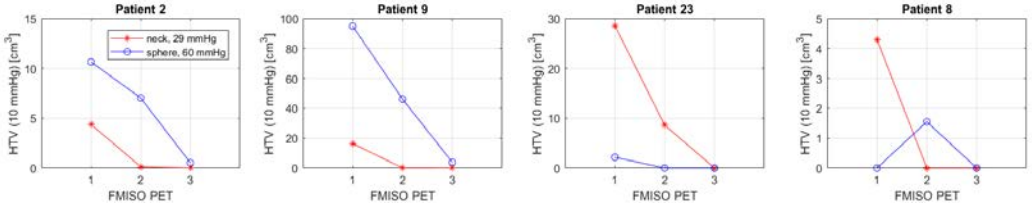


Figure 5.6: Evolution of HTV values during the treatment by using the uptake conversion model and as WOVs the deep neck muscle with 29 mmHg oxygenation reference and the shoulder region with 60 mmHg oxygenation reference.

show any disappearance of hypoxia along the treatment.
The use of the neck muscle with 29 mmHg reference and of the shoulder region with 60 mmHg reference as WOVs leads to about 70% agreement on the classification of the 30 patients as hypoxic or non-hypoxic. However, it should be mentioned that the volumes have different extensions and spatial localization; indeed, the DICE coefficient for the hypoxic volumes found with these two methods for FMISO PET 1 has a mean value of $0.16 \pm 0.21$, with a median of 0.05, indicating a poor spatial matching. Despite this, their evolution during the weeks of treatment are similar, with corresponding growths and decreases in most of the cases, as Fig. 5.6 depicts for some of the patients in the available dataset: even if with different magnitudes, the two methods have analog behaviors for instance in Patients 2, 9 and 23 (in total in 25 patients out of 30); in some case (5 patients out of 30), like for Patient 8, they present different trends. Overall the mean normalized cross-correlation coefficient for the 30 pairs of curves is $0.82 \pm 0.25$.

For what concerns the standard method, since the choice of a TMR $\geq 1.4$ does not seem to be suitable for this patient dataset, additional analysis was performed to study in detail this aspect. Interestingly, the HTV corresponding to TMR $\geq 1.4$ is not significantly similar to the volume contoured in the $pO_2$ map defined with the WOV located in the deep neck muscle with 29 mmHg as reference (DICE = $0.05 \pm 0.06$, median 0.02); still, they are significantly similar when the threshold for hypoxia is raised to 18 mmHg as median value for all the patients in the study (mean value equal to $18.0 \pm 0.5$ mmHg), instead of the standard hypoxia threshold of 10 mmHg (DICE = $0.79 \pm 0.17$, median 0.82). Fig. 5.7 makes this concept clear for one representative patient.

## 5.2 On the calculation of re-oxygenation functions

Firstly, an analysis of the influence of the binning of the data and of the method adopted for the fitting was done.

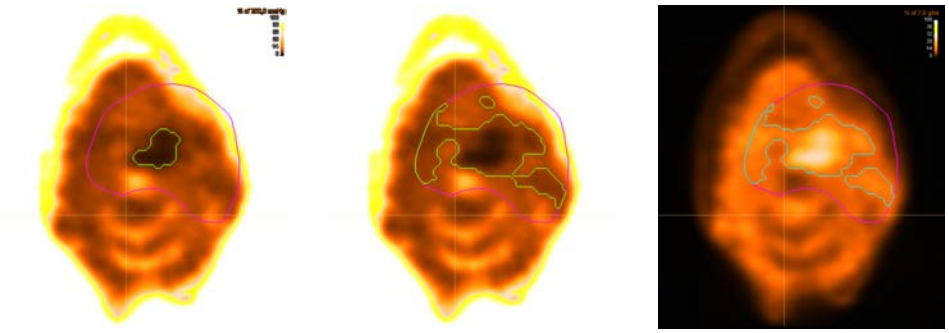

(a) (b) (c)

Figure 5.7: Similarity of volumes when changing the threshold for hypoxia (Patient 21); HN2 in magenta and HTV in green or light blue. Subfig. 5.7a shows the $pO_2$ map obtained by using the deep neck muscle as WOV and 29 mmHg as reference, while the standard threshold for hypoxia (10 mmHg) is maintained; Subfig. 5.7b represents the same map with a threshold for hypoxia raised to 18 mmHg; Subfig. 5.7c represent the FMISO PET 1 uptakes with the HTV defined by a TMR $\geq$ 1.4.

In particular, the binning of the $pO_2$ data (i.e. the choice of the bins width on the X axis of Fig. 5.8) contained in the expanded HTV has an influence when using the Least Squares method. The Least Squares method tries to find the best parameters of the given distribution, fitting the middle points of each bin by minimizing the sum of the squared residuals; therefore, a modification of the bins width leads to a shift of the bin centers and to different counts. The consequence is a variation in the parameters of the fitting distribution, as shown in Fig. 5.8. It may seem reasonable to apply this method when trying to fit a given distribution, because it gives the possibility to decide the level of "noise" of the data by choosing wider or narrower bins. But it is necessary to point out that the Least Squares method is exploitable when some basic requirements are fulfilled; in particular, for this fitting problem, the most relevant hypotheses to respect are the following three:

- measurement errors must be symmetric;
- along the distribution the variability must be the same;
- the measurements must be independent,

where with measurement it is intended the count for a specific bin. Here the three hypotheses are violated, because: first, the bin counts are non-negative and thus measurement errors are asymmetric, especially when the count is close to 0; second, the tails have different variability with respect to the center of the distribution; third, the bin counts, having a fixed sum, are not independent values.
For these reasons an alternative method, based on Maximum Likelihood, has been

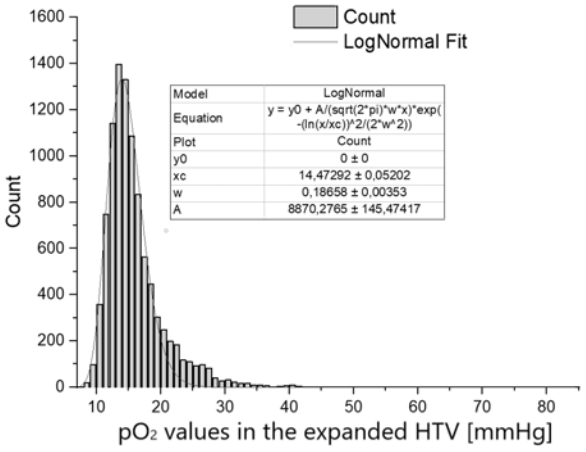


(a)

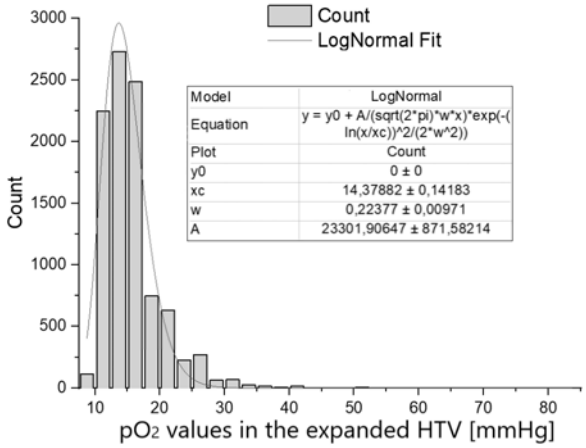


(b)

Figure 5.8: Impact of the choice of the bin width on the fitting parameters when using Least Squares (fitting with LogNormal distribution): 5.8a. Bin width=1 mmHg; 5.8b. Bin width=2.5 mmHg.

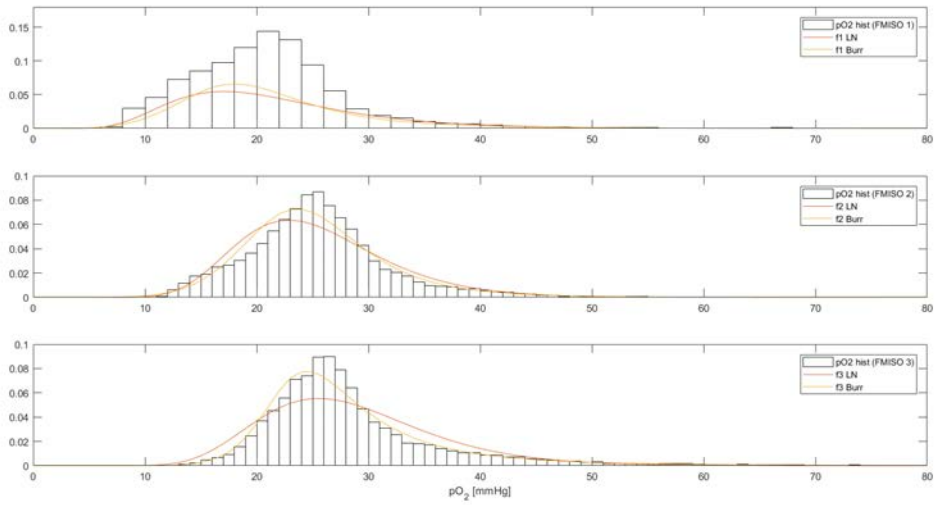


Figure 5.9: Normalized $pO_2$ histograms of the three maps and correspondent fitting curves (LogNormal and Burr) obtained with the Maximum Likelihood Estimation for the Patient 08.

considered. It does not present the issue of the binning of the data, as it estimates the parameters of the fitting distribution by adopting the raw data, instead of grouped data. Even though the results obtained are reliable, a possible drawback of this method is that the found curve might be noisier, as in the raw data can be present abrupt variations in the $pO_2$ distribution.
An example of the comparison between the fitting of the two distribution is represented in Fig. 5.9, where it can be visually inferred that the Burr distribution seems to fit the data better than the LogNormal. The mentioned increased "goodness" of fit is also reflected by a mean adjusted R-square value of 0.97 for the Burr distribution, versus a value of 0.85 for the Log-Normal.
It was shown that different functions used for fitting the histograms for $pO_2$ render different re-oxygenation functions characterized by different graphical representations, displayed for one patient in Fig. 5.10.

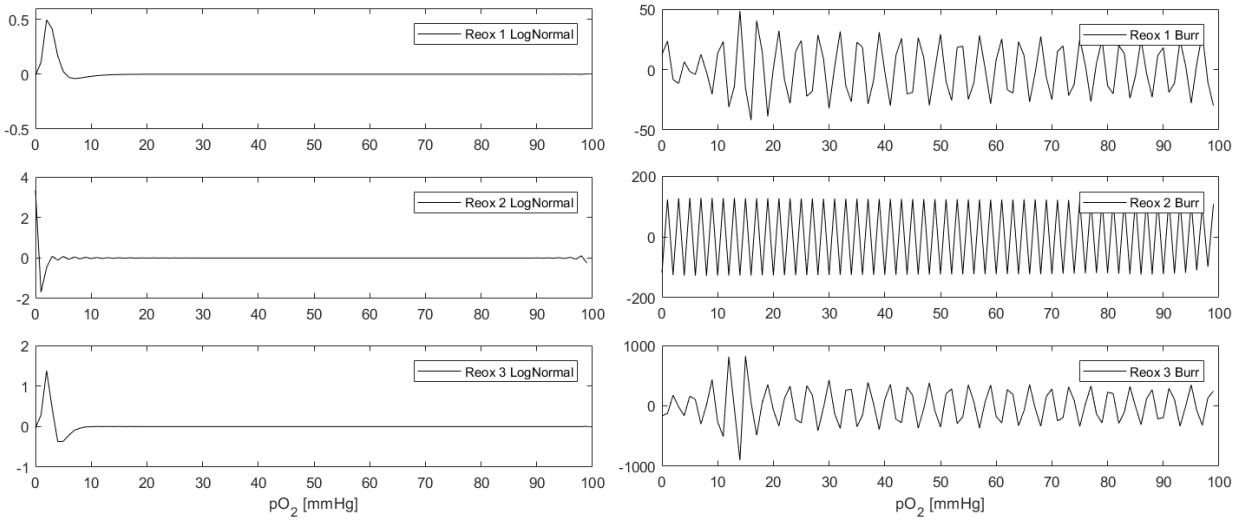


Figure 5.10: Representative re-oxygenation functions ($reox1$, $reox2$ and $reox3$) obtained after the use of two fitting distributions (LogNormal and Burr) of the $pO_2$ histograms.

# 6 Discussion

Hypoxia is one of the leading causes of failure of radiotherapy in head and neck cancer due to an increase in the cells radioresistance of a factor up to about three times [2]. The imaging of hypoxia in the last decade focused especially on the use of positron emission tomography; meanwhile $^{18}$F-FMISO has affirmed as the standard radiotracer for the purpose [3]. Many efforts have been put on the research of novel methods for the dose painting to the more radioresistant volumes in tumors, even though none of them has been officially introduced in the clinical routine.
The dose painting by contours has been widely acknowledged so far, giving straightforward techniques for the contouring of the hypoxic subvolumes based on a global threshold on the uptake values and for homogeneous escalated dose distribution. On the other hand, despite an easier dose boost implementation, the dose results uniform in the hypoxic target and not necessarily follows a biological map of the tumor radioresistance [74].
For some years, instead, a parallel path based on dose painting by numbers has revealed approaches relying on the radiobiological features of the tumor microenvironment. A recent FMISO uptake model allows to transfer values from the tracer uptake domain to the oxygen partial pressure one [4]; the obtained maps acquire biological meaning, with consequent better descriptions of the tumor microenvironment and the possibility of establishing functions of re-oxygenation, whenever multiple acquisitions during the treatment are available.
The present work wanted first of all to explore the influence of the choice of the Well-Oxygenated Volume and its reference value, in order to set the bases for the introduction of a standard method for the delineation of the hypoxic subvolumes. Secondly, the histograms related to the latters have been examined, aiming to find their best fitting distribution and subsequently define a finite set of possible re-oxygenation functions, carrying on a task explored in the past year for a restricted dataset of two patients (three lesions in total) [5].

For the definition of the hypoxic targets, the well-oxygenated regions studied were a sphere in the shoulder with a reference value of 60 mmHg and the posterior deep neck muscle with reference values of 29 mmHg and 60 mmHg, while a standard approach by thresholding at 1.4 the ratio between tumor and neck muscle uptakes was accounted for comparison.
The neck muscle with reference of 60 mmHg does not seem to be a reliable WOV, indeed only 2 patients out of 30 in the dataset result hypoxic, a fraction not met by histologic analyses.
Instead, the first two WOVs accord in a relevant fraction of the cases when it comes to establish whether a patient presents hypoxia or not; however the determination of the shoulder region is not univocal and often is not visible in the PET acquisitions for HNC.
Unfortunately these volumes do not agree with the standard method, since it classified all the patients as hypoxic with quite large volumes. Presumably the threshold

of 1.4 often adopted in clinical practice was not suitable for this patients' dataset. But a remarkable finding came from the comparison between the uptake volumes and one of the $pO_2$ maps, the one resulting from the choice of the posterior deep neck muscle with 29 mmHg as reference. Their associated hypoxic targets were indeed nearly matching in space, given the assumption of setting the threshold for hypoxia at 18 mmHg, instead of 10 mmHg. This may lead to draw two conclusions:

- that the normally used threshold of 1.4 for the TMR might be actually too conservative, being linked to an higher threshold for hypoxia than the standard 10 mmHg;
- that the uptake model for FMISO and for HNC gives volumes consistent with the conventional method, when the chosen WOV is the posterior deep neck muscle with a $pO_2$ reference value of 29 mmHg, even though a shift of the threshold for hypoxia was here necessary.

It was shown that the mathematical expression of the different functions used for the fitting of the oxygen distribution expressed as histograms has a high influence on the graphical representation of the re-oxygenation function. This result is warranting further investigations with respect to the interpretation of the shapes of the different re-oxygenation functions both in terms of signal processing, but also in terms of the physiological underlining processes. The results should, however, be put into the boarder context of the overall aim of the study, namely finding one (or several) mathematical description for the re-oxygenation functions, reproducible and robust to variations in the original shape of the histograms, characterized by sets of parameters that correlate with the clinical observations and hence that could be used for making predictions regarding the treatment outcome. The accuracy of these function with respect to the original fitting is not a critical issue as long as the pattern of response could be predicted based on their shapes or parameters.

# 7 Conclusions

Hypoxic tumors make the delivery of radiation therapies less effective; the dose painting to the hypoxic subvolumes is required to increase the tumor control. The FMISO uptake model proposed by Toma-Dasu is useful to describe the radioresistance of the cancer tissues as a map of $pO_2$ values, with which it is possible to boost the dose to the cells more reluctant to eradication. However, in this context a reference oxygenated tissue needs to be chosen and the present thesis showed how the choice of the WOV and its reference value are crucial for the representation of the final oxygen partial pressure map. A good candidate reference for HNC has been found in the posterior deep neck muscle, when assigning to it a $pO_2$ equal to 29 mmHg. The goodness of this choice has been determined by a comparison with a method currently considered a standard for the contouring of hypoxia in HNC and derived from the literature, that is the use of a threshold equal to 1.4 on the tumor-to-muscle ratio, where the muscle considered is generally the neck muscle. Nevertheless, further efforts should be put on understanding to which threshold for hypoxia the standard method is corresponding, as from the analyses here conducted it seems to correspond to a threshold of 18 mmHg, almost double with respect to the one general assumed, 10 mmHg.
Conscious of the fact that these considerations lay on a quite rich dataset for a single study and could have a certain impact on the current scene, they clearly deserve to be confirmed by other centers of research, repeating similar results in analogous conditions, before final conclusions on the subject could be drawn and possible clinical trials with dose painting delivered with the aid of the presented method could start.
The re-oxygenation functions found with the method proposed by Lazzeroni et al. have shapes depending on the distribution used to fit the histograms containing the $pO_2$ values in the neighborhood of the hypoxic volumes. Further research is needed for understanding the correlation between the shapes or parameters of such functions and the outcome of the therapy.

# References


[1] B.-J. Hong, J. Kim, H. Jeong, S. Bok, Y.-E. Kim, and G.-O. Ahn, "Tumor hypoxia and reoxygenation: the yin and yang for radiotherapy," *Radiation Oncology Journal*, vol. 34, no. 4, pp. 239–249, 2016.

[2] S. Rockwell, I. T. Dobrucki, E. Y. Kim, S. T. Marrison, and T. van Vu, "Hypoxia and radiation therapy: Past history, ongoing research, and future promise," *Current Molecular Medicine*, vol. 9, no. 4, pp. 442–458, 2009.

[3] K. A. Krohn, J. M. Link, and R. P. Mason, "Molecular imaging of hypoxia," *The Journal of Nuclear Medicine*, no. 49, pp. 129–148, 2008.

[4] I. Toma-Dasu, J. Uhrdin, A. Daşu, and A. Brahme, "Therapy optimization based on non-linear uptake of pet tracers versus "linear dose painting"," in *World Congress on Medical Physics and Biomedical Engineering, September 7 - 12, 2009, Munich, Germany* (O. Dössel and W. C. Schlegel, eds.), (Berlin, Heidelberg), pp. 221–224, Springer Berlin Heidelberg, 2009.

[5] M. Lazzeroni, H. Bunea, A. L. Grosu, D. Baltas, I. Toma-Dasu, and A. Dasu, "Mathematical description of changes in tumour oxygenation from repeated functional imaging," *Advances in Experimental Medicine and Biology [Accepted for publication]*, no. 1072, 2018.

[6] National Cancer Istitute, "https://www.cancer.gov/publications/dictionaries/cancer-terms/def/tumor: Nci dictionary of cancer terms - tumor."

[7] National Cancer Istitute, "https://www.cancer.gov/publications/dictionaries/cancer-terms/def/cancer: Nci dictionary of cancer terms - cancer."

[8] A. Kułakowski, "The contribution of marie skłodowska-curie to the development of modern oncology," *Analytical and Bioanalytical Chemistry*, no. 400, pp. 1583–1586, 2011.

[9] J. R. Hubenak, Q. Zhang, C. D. Branch, and S. J. Kronowitz, "Mechanisms of injury to normal tissue after radiotherapy: a review," *Plastic and Reconstructive Surgery*, vol. 133, no. 1, pp. 49e–56e, 2014.

[10] M. Joiner and A. ven der Kogel, *Basic Clinical Radiobiology*. Hodder Arnold, 4th ed., 2009.

[11] M. Beyzadeoglu, G. Ozyigit, and C. Ebruli, *Basic radiation oncology*. Springer, 2010.

[12] E. K. Lindblom, *Time, dose and fractionation: accounting for hypoxia in the search for optimal radiotherapy treatment parameters*. Doctoral thesis, Stockholm University, Sweden, 2017.

[13] D. S. Chang, F. D. Lasley, I. J. Das, M. S. Mendonca, and J. R. Dynlacht, "Therapeutic ratio," in *Basic Radiotherapy Physics and Biology*, pp. 277–282, Cham: Springer International Publishing, 2014.

[14] M. Nordsmark, S. M. Bentzen, V. Rudat, D. Brizel, E. Lartigau, P. Stadler, A. Becker, M. Adam, M. Molls, J. Dunst, D. J. Terris, and J. Overgaard, "Prognostic value of tumor oxygenation in 397 head and neck tumors after primary radiation therapy. an international multi-center study.," *Radiotherapy and Oncology*, vol. 77, no. 1, pp. 18–24, 2005.

[15] R. H. Thomlinson and L. H. Gray, "The histological structure of some human lung cancers and the possible implications implications for radiotherapy," *Br J Cancer*, vol. 9, no. 4, pp. 539–549, 1955.

[16] C. Bayer, K. Shi, S. T. Astner, C.-A. Maftei, and P. Vaupel, "Acute versus chronic hypoxia: why a simplified classification is not enough," *International Journal of Radiation Oncology Biology Physics*, vol. 80, no. 4, pp. 965–968, 2011.

[17] C. Bayer and P. Vaupel, "Acute versus chronic hypoxia in tumors: Controversial data concerning time frames and biological consequences," *Strahlentherapie und Onkologie*, no. 188, pp. 616–627, 2012.

[18] A. Carreau, B. E. Hafny-Rahbi, A. Matejuk, C. Grillon, and C. Kieda, "Why is the partial oxygen pressure of human tissues a crucial parameter? small molecules and hypoxia," *Journal of Cellular and Molecular Medicine*, vol. 15, no. 6, pp. 1239–1253, 2011.

[19] S. E. Rademakers, P. N. Span, J. H. A. M. Kaanders, F. C. G. J. Sweep, A. J. van der Kogel, and J. Bussink, "Molecular aspects of tumour hypoxia," *Molecular Oncology*, no. 2, pp. 41–53, 2008.

[20] J. Overgaard, "Hypoxic radiosensitization: Adored and ignored," *Journal of Clinical Oncology*, vol. 25, no. 26, pp. 4066–4074, 2007.

[21] M. R. Horsman and J. Overgaard, "The impact of hypoxia and its modification of the outcome of radiotherapy," *Journal of Radiation Research*, vol. 57, no. Suppl 1, pp. i90–8, 2016.

[22] C. M. Hoff, P. Lassen, J. G. Eriksen, H. S. Hansen, L. Specht, M. Overgaard, C. Grau, J. Johansen, J. Bentzen, L. Andersen, J. F. Evensen, and J. Overgaard, "Does transfusion improve the outcome for hnscc patients treated with radiotherapy? – results from the randomized dahanca 5 and 7 trials," *Acta Oncologica*, vol. 50, no. 7, pp. 1006–1014, 2011.

[23] L. Welsh, R. Panek, A. Riddell, K. Wong, M. O. Leach, M. Tavassoli, D. Rahman, M. Schmidt, T. Hurley, L. Grove, T. Richards, D.-M. Koh, C. Nutting, K. Harrington, K. Newbold, and S. Bhide, "Blood transfusion during radical

chemo-radiotherapy does not reduce tumour hypoxia in squamous cell cancer of the head and neck," *Br J Cancer*, vol. 116, no. 1, pp. 28–35, 2017.

[24] T. Wenzl and J. J. Wilkens, "Theoretical analysis of the dose dependence of the oxygen enhancement ratio and its relevance for clinical applications," *Radiation Oncology*, vol. 171, no. 6, 2011.

[25] I. Toma-Dasu and A. Dasu, "Modelling tumour oxygenation, reoxygenation and implications on treatment outcome," *Computational and Mathematical Methods in Medicine*, vol. 2013, 2013.

[26] S. Vallabhajosula, "18f-labeled positron emission tomographic radiopharmaceuticals in oncology: An overview of radiochemistry and mechanism of tumor localization," *Seminars in nuclear medicine*, no. 37, pp. 400–419, 2007.

[27] S. Vallabhajosula, *Molecular Imaging: Radiopharmaceuticals for PET and SPECT*. Springer Berlin Heidelberg, 2009.

[28] J. D. Chapman, "The detection and measurement of hypoxic cells in solid tumors," *Cancer*, no. 54, pp. 2441–2449, 1984.

[29] R. Blasberg, M. Horowitz, J. Strong, P. Molnar, C. Patlak, E. Owens, and J. Fenstermacher, "Regional measurements of [14c]misonidazole distribution and blood flow in subcutaneous rt-9 experimental tumors," *Cancer Research*, 1985.

[30] J. S. Rasey, Z. Grunbaum, S. Magee, N. J. Nelson, P. L. Olive, R. E. Durand, and K. A. Krohn, "Characterization of radiolabeled fluoromisonidazole as a probe for hypoxic cells," *Radiation Research*, vol. 111, no. 2, pp. 292–304, 1987.

[31] O. Couturier, A. Luxen, J. F. Chatal, J. P. Vuillez, P. Rigo, and R. Hustinx, "Fluorinated tracers for imaging cancer with positron emission tomography.," *European Journal of Nuclear Medicine and Molecular Imaging*, vol. 31, no. 8, pp. 1182–1206, 2004.

[32] E. Lopci, I. Grassi, A. Chiti, C. Nanni, G. Cicoria, L. Toschi, C. Fonti, F. Lodi, S. Mattioli, and S. Fanti, "Pet radiopharmaceuticals for imaging of tumor hypoxia: a review of the evidence," *American Journal of Nuclear Medicine and Molecular Imaging*, vol. 4, no. 4, pp. 365–384, 2014.

[33] L. J. Dubois, N. G. Lieuwes, M. H. M. Janssen, W. J. M. Peeters, A. D. Windhorst, J. C. Walsh, H. C. Kolb, M. C. Öllers, J. Bussink, van Dongen, Guus A M S, A. van der Kogel, and P. Lambin, "Preclinical evaluation and validation of (18)fhx4, a promising hypoxia marker for pet imaging," *Proceedings of the National Academy of Sciences of the United States of America*, vol. 108, no. 35, pp. 14620–14625, 2011.

[34] S. G. J. A. Peeters, C. M. L. Zegers, N. G. Lieuwes, W. van Elmpt, J. Eriksson, G. A. M. S. van Dongen, L. Dubois, and P. Lambin, "A comparative study of the hypoxia pet tracers [18f]hx4, [18f]faza, and [18f]fmiso in a preclinical tumor model," *International Journal of Radiation Oncology*Biology*Physics*, vol. 91, no. 2, pp. 351–359, 2015.

[35] L. Chen, Z. Zhang, H. C. Kolb, J. C. Walsh, J. Zhang, and Y. Guan, "18f-hx4 hypoxia imaging with pet/ct in head and neck cancer: a comparison with 18f-fmiso," *Nuclear Medicine Communications*, vol. 33, no. 10, 2012.

[36] B. Henriques de Figueiredo, T. Merlin, H. de Clermont-Gallerande, M. Hatt, D. Vimont, P. Fernandez, and F. Lamare, "Potential of 18f-fluoromisonidazole positron-emission tomography for radiotherapy planning in head and neck squamous cell carcinomas," *Strahlentherapie und Onkologie: Organ der Deutschen Rontgengesellschaft*, vol. 189, no. 12, pp. 1015–1019, 2013.

[37] Sarah G.J.A. Peeters, Catharina M.L. Zegers, Natasja G. Lieuwes, Wouter van Elmpt, Jonas Eriksson, Guus A.M.S. van Dongen, Ludwig Dubois, and Philippe Lambin, "A comparative study of the hypoxia pet tracers [18f]hx4, [18f]faza, and [18f]fmiso in a preclinical tumor model," *International Journal of Radiation Oncology*Biology*Physics*, vol. 91, no. 2, pp. 351–359, 2015.

[38] I. Toma-Dasu, J. Uhrdin, L. Antonovic, A. Dasu, S. Nuyts, P. Dirix, K. Haustermans, and A. Brahme, "Dose prescription and treatment planning based on fmiso-pet hypoxia," *Acta Oncologica*, vol. 51, no. 2, pp. 222–230, 2012.

[39] M. Kikuchi, T. Yamane, S. Shinohara, K. Fujiwara, S.-y. Hori, Y. Tona, H. Yamazaki, Y. Naito, and M. Senda, "18f-fluoromisonidazole positron emission tomography before treatment is a predictor of radiotherapy outcome and survival prognosis in patients with head and neck squamous cell carcinoma," *Annals of nuclear medicine*, vol. 25, no. 9, pp. 625–633, 2011.

[40] J. Sato, Y. Kitagawa, Y. Yamazaki, H. Hata, T. Asaka, M. Miyakoshi, S. Okamoto, T. Shiga, M. Shindoh, Y. Kuge, and N. Tamaki, "Advantage of fmiso-pet over fdg-pet for predicting histological response to preoperative chemotherapy in patients with oral squamous cell carcinoma," *European Journal of Nuclear Medicine and Molecular Imaging*, vol. 41, no. 11, pp. 2031–2041, 2014.

[41] J. Sato, Y. Kitagawa, S. Watanabe, T. Asaka, N. Ohga, K. Hirata, S. Okamoto, T. Shiga, M. Shindoh, Y. Kuge, and N. Tamaki, "(18)f-fluoromisonidazole positron emission tomography (fmiso-pet) may reflect hypoxia and cell proliferation activity in oral squamous cell carcinoma," *Oral surgery, oral medicine, oral pathology and oral radiology*, vol. 124, no. 3, pp. 261–270, 2017.

[42] U. Simoncic, S. Leibfarth, S. Welz, N. Schwenzer, H. Schmidt, G. Reischl, C. Pfannenberg, C. La Fougere, K. Nikolaou, D. Zips, and D. Thorwarth, "Comparison of dce-mri kinetic parameters and fmiso-pet uptake parameters in head and neck cancer patients," *Medical physics*, vol. 44, no. 6, pp. 2358–2368, 2017.

[43] S. Okamoto, T. Shiga, K. Yasuda, Y. M. Ito, K. Magota, K. Kasai, Y. Kuge, H. Shirato, and N. Tamaki, "High reproducibility of tumor hypoxia evaluated by 18f-fluoromisonidazole pet for head and neck cancer," *Journal of nuclear medicine : official publication, Society of Nuclear Medicine*, vol. 54, no. 2, pp. 201–207, 2013.

[44] S. M. Eschmann, F. Paulsen, C. Bedeshem, H.-J. Machulla, T. Hehr, M. Bamberg, and R. Bares, "Hypoxia-imaging with (18)f-misonidazole and pet: changes of kinetics during radiotherapy of head-and-neck cancer," *Radiotherapy and oncology : journal of the European Society for Therapeutic Radiology and Oncology*, vol. 83, no. 3, pp. 406–410, 2007.

[45] Y. Nishikawa, K. Yasuda, S. Okamoto, Y. M. Ito, R. Onimaru, T. Shiga, K. Tsuchiya, S. Watanabe, W. Takeuchi, Y. Kuge, H. Peng, N. Tamaki, and H. Shirato, "Local relapse of nasopharyngeal cancer and voxel-based analysis of fmiso uptake using pet with semiconductor detectors," *Radiation oncology (London, England)*, vol. 12, no. 1, p. 148, 2017.

[46] M. Grkovski, N. Y. Lee, H. Schoder, S. D. Carlin, B. J. Beattie, N. Riaz, J. E. Leeman, J. A. O'Donoghue, and J. L. Humm, "Monitoring early response to chemoradiotherapy with (18)f-fmiso dynamic pet in head and neck cancer," *European Journal of Nuclear Medicine and Molecular Imaging*, vol. 44, no. 10, pp. 1682–1691, 2017.

[47] S.-M. Eschmann, F. Paulsen, M. Reimold, H. Dittmann, S. Welz, G. Reischl, H.-J. Machulla, and R. Bares, "Prognostic impact of hypoxia imaging with 18f-misonidazole pet in non-small cell lung cancer and head and neck cancer before radiotherapy," *Journal of nuclear medicine : official publication, Society of Nuclear Medicine*, vol. 46, no. 2, pp. 253–260, 2005.

[48] S. Okamoto, T. Shiga, K. Yasuda, S. Watanabe, K. Hirata, K.-I. Nishijima, K. Magota, K. Kasai, R. Onimaru, K. Tuchiya, Y. Kuge, H. Shirato, and N. Tamaki, "The reoxygenation of hypoxia and the reduction of glucose metabolism in head and neck cancer by fractionated radiotherapy with intensity-modulated radiation therapy," *European Journal of Nuclear Medicine and Molecular Imaging*, vol. 43, no. 12, pp. 2147–2154, 2016.

[49] D. Monnich, D. Thorwarth, S. Leibfarth, C. Pfannenberg, G. Reischl, P.-S. Mauz, K. Nikolaou, C. La Fougere, D. Zips, and S. Welz, "Overlap of highly fdg-avid and fmiso hypoxic tumor subvolumes in patients with head and neck cancer," *Acta oncologica (Stockholm, Sweden)*, vol. 56, no. 11, pp. 1577–1582, 2017.

[50] D. Zips, K. Zophel, N. Abolmaali, R. Perrin, A. Abramyuk, R. Haase, S. Appold, J. Steinbach, J. Kotzerke, and M. Baumann, "Exploratory prospective trial of hypoxia-specific pet imaging during radiochemotherapy in patients with locally advanced head-and-neck cancer," *Radiotherapy and oncology : journal of the European Society for Therapeutic Radiology and Oncology*, vol. 105, no. 1, pp. 21–28, 2012.

[51] M. Zimny, B. Gagel, E. DiMartino, K. Hamacher, H. H. Coenen, M. Westhofen, M. Eble, U. Buell, and P. Reinartz, "Fdg–a marker of tumour hypoxia? a comparison with 18ffluoromisonidazole and po2-polarography in metastatic head and neck cancer," *European Journal of Nuclear Medicine and Molecular Imaging*, vol. 33, no. 12, pp. 1426–1431, 2006.

[52] M. B. Barton, M. Frommer, and J. Shafiq, "Role of radiotherapy in cancer control in low-income and middle-income countries," *The Lancet. Oncology*, vol. 7, no. 7, pp. 584–595, 2006.

[53] M. B. Barton, S. Jacob, J. Shafiq, K. Wong, S. R. Thompson, T. P. Hanna, and G. P. Delaney, "Estimating the demand for radiotherapy from the evidence: a review of changes from 2003 to 2012," *Radiotherapy and oncology : journal of the European Society for Therapeutic Radiology and Oncology*, vol. 112, no. 1, pp. 140–144, 2014.

[54] N. Vigneswaran and M. D. Williams, "Epidemiologic trends in head and neck cancer and aids in diagnosis," *Oral and maxillofacial surgery clinics of North America*, vol. 26, no. 2, pp. 123–141, 2014.

[55] A. Saadeddin, "Radiotherapy for nsclc: review of conventional and new treatment techniques," *Journal of infection and public health*, vol. 5 Suppl 1, pp. S45–9, 2012.

[56] M. Teoh, C. H. Clark, K. Wood, S. Whitaker, and A. Nisbet, "Volumetric modulated arc therapy: a review of current literature and clinical use in practice," *The British Journal of Radiology*, no. 84, pp. 967–996, 2011.

[57] L. Ma, L. Wang, C.-L. Tseng, and A. Sahgal, "Emerging technologies in stereotactic body radiotherapy," *Chinese Clinical Oncology*, vol. 6, no. 2, 2017.

[58] N. G. Burnet, S. J. Thomas, K. E. Burton, and S. J. Jefferies, "Defining the tumour and target volumes for radiotherapy," *Cancer Imaging*, vol. 4, no. 2, pp. 153–161, 2004.

[59] A. K. Berthelsen, J. Dobbs, E. Kjellén, T. Landberg, T. R. Möller, P. Nilsson, L. Specht, and A. Wambersie, "What's new in target volume definition for radiologists in icru report 71? how can the icru volume definitions be integrated in clinical practice?," *Cancer Imaging*, vol. 7, no. 1, pp. 104–116, 2007.

[60] I. Tachibana, Y. Nishimura, T. Shibata, S. Kanamori, K. Nakamatsu, R. Koike, T. Nishikawa, K. Ishikawa, M. Tamura, and M. Hosono, "A prospective clinical trial of tumor hypoxia imaging with 18f-fluoromisonidazole positron emission tomography and computed tomography (f-miso pet/ct) before and during radiation therapy," *Journal of Radiation Research*, vol. 54, no. 6, pp. 1078–1084, 2013.

[61] N. E. Wiedenmann, S. Bucher, M. Hentschel, M. Mix, W. Vach, M.-I. Bittner, U. Nestle, J. Pfeiffer, W. A. Weber, and A. L. Grosu, "Serial 18f-fluoromisonidazole pet during radiochemotherapy for locally advanced head and neck cancer and its correlation with outcome," *Radiotherapy and oncology : journal of the European Society for Therapeutic Radiology and Oncology*, vol. 117, no. 1, pp. 113–117, 2015.

[62] J. G. Rajendran, D. L. Schwartz, J. O'Sullivan, L. M. Peterson, P. Ng, J. Scharnhorst, J. R. Grierson, and K. A. Krohn, "Tumor hypoxia imaging with f-18 fluoromisonidazole positron emission tomography in head and neck cancer," *Clinical cancer research : an official journal of the American Association for Cancer Research*, vol. 12, no. 18, pp. 5435–5441, 2006.

[63] S. Welz, D. Monnich, C. Pfannenberg, K. Nikolaou, M. Reimold, C. La Fougere, G. Reischl, P.-S. Mauz, F. Paulsen, M. Alber, C. Belka, D. Zips, and D. Thorwarth, "Prognostic value of dynamic hypoxia pet in head and neck cancer: Results from a planned interim analysis of a randomized phase ii hypoxia-image guided dose escalation trial," *Radiotherapy and oncology : journal of the European Society for Therapeutic Radiology and Oncology*, vol. 124, no. 3, pp. 526–532, 2017.

[64] S. Lock, R. Perrin, A. Seidlitz, A. Bandurska-Luque, S. Zschaeck, K. Zophel, M. Krause, J. Steinbach, J. Kotzerke, D. Zips, E. G. C. Troost, and M. Baumann, "Residual tumour hypoxia in head-and-neck cancer patients undergoing primary radiochemotherapy, final results of a prospective trial on repeat fmiso-pet imaging," *Radiotherapy and oncology : journal of the European Society for Therapeutic Radiology and Oncology*, vol. 124, no. 3, pp. 533–540, 2017.

[65] S. A. Nehmeh, N. Y. Lee, H. Schroder, O. Squire, P. B. Zanzonico, Y. E. Erdi, C. Greco, G. Mageras, H. S. Pham, S. M. Larson, C. C. Ling, and J. L. Humm, "Reproducibility of intratumor distribution of (18)f-fluoromisonidazole in head and neck cancer," *International Journal of Radiation Oncology*Biology*Physics*, vol. 70, no. 1, pp. 235–242, 2008.

[66] N. Tamaki and K. Hirata, "Tumor hypoxia: a new pet imaging biomarker in clinical oncology," *International journal of clinical oncology*, vol. 21, no. 4, pp. 619–625, 2016.

[67] D. Monnich, E. G. C. Troost, Kaanders, Johannes H A M, W. J. G. Oyen, M. Alber, and D. Thorwarth, "Modelling and simulation of the influence of

acute and chronic hypoxia on 18ffluoromisonidazole pet imaging," *Physics in medicine and biology*, vol. 57, no. 6, pp. 1675–1684, 2012.

[68] M.-I. Bittner, N. Wiedenmann, S. Bucher, M. Hentschel, M. Mix, W. A. Weber, and A.-L. Grosu, "Exploratory geographical analysis of hypoxic subvolumes using 18f-miso-pet imaging in patients with head and neck cancer in the course of primary chemoradiotherapy," *Radiotherapy and oncology : journal of the European Society for Therapeutic Radiology and Oncology*, vol. 108, no. 3, pp. 511–516, 2013.

[69] M.-I. Bittner and A.-L. Grosu, "Hypoxia in head and neck tumors: Characteristics and development during therapy," *Frontiers in Oncology*, vol. 3, 2013.

[70] S. Zschaeck, R. Haase, N. Abolmaali, R. Perrin, K. Stutzer, S. Appold, J. Steinbach, J. Kotzerke, D. Zips, C. Richter, V. Gudziol, M. Krause, K. Zophel, and M. Baumann, "Spatial distribution of fmiso in head and neck squamous cell carcinomas during radio-chemotherapy and its correlation to pattern of failure," *Acta oncologica (Stockholm, Sweden)*, vol. 54, no. 9, pp. 1355–1363, 2015.

[71] L. S. Mortensen, J. Johansen, J. Kallehauge, H. Primdahl, M. Busk, P. Lassen, J. Alsner, B. S. Sorensen, K. Toustrup, S. Jakobsen, J. Petersen, H. Petersen, J. Theil, M. Nordsmark, and J. Overgaard, "Faza pet/ct hypoxia imaging in patients with squamous cell carcinoma of the head and neck treated with radiotherapy: results from the dahanca 24 trial," *Radiotherapy and oncology : journal of the European Society for Therapeutic Radiology and Oncology*, vol. 105, no. 1, pp. 14–20, 2012.

[72] T. Saga, M. Inubushi, M. Koizumi, K. Yoshikawa, M.-R. Zhang, T. Obata, K. Tanimoto, R. Harada, T. Uno, and Y. Fujibayashi, "Prognostic value of pet/ct with (18)f-fluoroazomycin arabinoside for patients with head and neck squamous cell carcinomas receiving chemoradiotherapy," *Annals of nuclear medicine*, vol. 30, no. 3, pp. 217–224, 2016.

[73] D. Thorwarth, S.-M. Eschmann, J. Scheiderbauer, F. Paulsen, and M. Alber, "Kinetic analysis of dynamic 18f-fluoromisonidazole pet correlates with radiation treatment outcome in head-and-neck cancer," *BMC cancer*, vol. 5, p. 152, 2005.

[74] D. R. Grimes, D. R. Warren, and S. Warren, "Hypoxia imaging and radiotherapy: bridging the resolution gap," *The British Journal of Radiology*, vol. 90, no. 1076, p. 20160939, 2017.

[75] J. H. Chang, M. Wada, N. J. Anderson, D. Lim Joon, S. T. Lee, S. J. Gong, D. H. Gunawardana, J. Sachinidis, G. O'Keefe, H. K. Gan, V. Khoo, and A. M. Scott, "Hypoxia-targeted radiotherapy dose painting for head and neck

cancer using (18)f-fmiso pet: a biological modeling study," *Acta oncologica (Stockholm, Sweden)*, vol. 52, no. 8, pp. 1723–1729, 2013.

[76] W. Choi, S.-w. Lee, S. H. Park, J. S. Ryu, S. J. Oh, K. C. Im, E. K. Choi, J. H. Kim, S. H. Jung, S. Kim, and S. D. Ahn, "Planning study for available dose of hypoxic tumor volume using fluorine-18-labeled fluoromisonidazole positron emission tomography for treatment of the head and neck cancer," *Radiotherapy and oncology : journal of the European Society for Therapeutic Radiology and Oncology*, vol. 97, no. 2, pp. 176–182, 2010.

[77] B. Henriques de Figueiredo, C. Zacharatou, S. Galland-Girodet, J. Benech, H. de Clermont-Gallerande, F. Lamare, M. Hatt, L. Digue, De Mones del Pujol, E, and P. Fernandez, "Hypoxia imaging with 18f-fmiso-pet for guided dose escalation with intensity-modulated radiotherapy in head-and-neck cancers," *Strahlentherapie und Onkologie : Organ der Deutschen Rontgengesellschaft ... [et al]*, vol. 191, no. 3, pp. 217–224, 2015.

[78] N. Y. Lee, J. G. Mechalakos, S. Nehmeh, Z. Lin, O. D. Squire, S. Cai, K. Chan, P. B. Zanzonico, C. Greco, C. C. Ling, J. L. Humm, and H. Schöder, "Fluorine-18-labeled fluoromisonidazole positron emission and computed tomography-guided intensity-modulated radiotherapy for head and neck cancer: A feasibility study," *International Journal of Radiation Oncology*Biology*Physics*, vol. 70, no. 1, pp. 2–13, 2008.

[79] S. Boeke, D. Thorwarth, D. Monnich, C. Pfannenberg, G. Reischl, C. La Fougere, K. Nikolaou, P.-S. Mauz, F. Paulsen, D. Zips, and S. Welz, "Geometric analysis of loco-regional recurrences in relation to pre-treatment hypoxia in patients with head and neck cancer," *Acta oncologica (Stockholm, Sweden)*, vol. 56, no. 11, pp. 1571–1576, 2017.

[80] K. S. Chao, W. R. Bosch, S. Mutic, J. S. Lewis, F. Dehdashti, M. A. Mintun, J. F. Dempsey, C. A. Perez, J. A. Purdy, and M. J. Welch, "A novel approach to overcome hypoxic tumor resistance: Cu-atsm-guided intensity-modulated radiation therapy," *International Journal of Radiation Oncology*Biology*Physics*, vol. 49, no. 4, pp. 1171–1182, 2001.

[81] S. Servagi-Vernat, S. Differding, F.-X. Hanin, D. Labar, A. Bol, J. A. Lee, and V. Gregoire, "A prospective clinical study of 18f-faza pet-ct hypoxia imaging in head and neck squamous cell carcinoma before and during radiation therapy," *European Journal of Nuclear Medicine and Molecular Imaging*, vol. 41, no. 8, pp. 1544–1552, 2014.

[82] P. Dirix, V. Vandecaveye, F. de Keyzer, S. Stroobants, R. Hermans, and S. Nuyts, "Dose painting in radiotherapy for head and neck squamous cell carcinoma: value of repeated functional imaging with (18)f-fdg pet, (18)f-fluoromisonidazole pet, diffusion-weighted mri, and dynamic contrast-enhanced mri," *Journal of nuclear medicine : official publication, Society of Nuclear Medicine*, vol. 50, no. 7, pp. 1020–1027, 2009.

[83] D. Thorwarth, S.-M. Eschmann, F. Paulsen, and M. Alber, "A model of reoxygenation dynamics of head-and-neck tumors based on serial 18f-fluoromisonidazole positron emission tomography investigations," *International Journal of Radiation Oncology*Biology*Physics*, vol. 68, no. 2, pp. 515–521, 2007.

[84] W. Wang, N. Y. Lee, J.-C. Georgi, M. Narayanan, J. Guillem, H. Schoder, and J. L. Humm, "Pharmacokinetic analysis of hypoxia (18)f-fluoromisonidazole dynamic pet in head and neck cancer," *Journal of nuclear medicine : official publication, Society of Nuclear Medicine*, vol. 51, no. 1, pp. 37–45, 2010.

[85] D. Thorwarth, S.-M. Eschmann, F. Paulsen, and M. Alber, "Hypoxia dose painting by numbers: a planning study," *International journal of radiation oncology, biology, physics*, vol. 68, no. 1, pp. 291–300, 2007.

[86] RaySearch Laboratories, "Deformable registration in raystation."

[87] Rafael García-Mollá, Noelia de Marco-Blancas, Jorge Bonaque, Laura Vidueira, Juan López-Tarjuelo, and José Perez-Calatayud, "Validation of a deformable image registration produced by a commercial treatment planning system in head and neck," *Physica Medica*, vol. 31, no. 3, pp. 219–223, 2015.